Tracing marine cryptotephras in the North Atlantic during the Last Glacial Period: Identification, characterisation and depositional controls

Peter M. Abbott[1,2,3,*], Adam J. Griggs[1], Anna J. Bourne[1,4], Siwan M. Davies[1]

[1]Department of Geography, College of Science, Swansea University, Singleton Park, Swansea, SA2 8PP, UK
[2]School of Earth and Ocean Sciences, Cardiff University, Park Place, CF10 3AT, Cardiff, UK
[3]Institute of Geological Sciences and Oeschger Center for Climate Change Research, University of Bern, Baltzerstrasse 1+3, Bern 3012, Switzerland
[4]Geography and Environment, University of Southampton, University Road, Southampton, SO17 1BJ, UK

*Corresponding author (abbottp@cardiff.ac.uk)

Abstract

Tephrochronology is increasingly being utilised as a key tool for improving chronological models and correlating disparate palaeoclimatic sequences. For many sedimentary environments, however, there is an increased recognition that a range of processes may impart a delay in deposition and/or rework tephra. These processes can affect the integrity of tephra deposits as time-synchronous markers, therefore, it is crucial to assess their isochronous nature, especially when cryptotephras are investigated in a dynamic marine environment. A methodology for the identification and characterisation of marine cryptotephras alongside a protocol for assessing their integrity is outlined. This was applied to a wide network of North Atlantic marine sequences covering the last glacial period. A diverse range of cryptotephra deposits were identified and based on similarities in physical characteristics, indicative of common modes of tephra delivery and post-depositional reworking, a deposit type classification scheme was defined. The presence and dominance of different deposit types within each core allowed an assessment of spatial and temporal controls on tephra deposition and preservation. Overall, isochronous horizons can be identified across a large portion of the North Atlantic due to preferential atmospheric dispersal patterns. However, the variable influence of ice-rafting processes and an interplay between the high eruptive frequency of Iceland and relatively lower sedimentation rates can also create complex tephrostratigraphies in this sector. We show that sites within a wide sector to the south and east of Iceland have the greatest potential to be repositories for isochronous horizons that can underpin or facilitate the synchronisation of palaeoclimatic records.

Keywords: Quaternary; palaeoceanography; tephrochronology; North Atlantic; transport and deposition; marine cores

1. Introduction

Deposits of volcanic ash, tephra, can act as time-synchronous marker horizons linking palaeoclimatic sequences to help improve chronological models and assess the relative timing of climatic changes (Lowe, 2011). Two fundamental principles that underpin the application of tephrochronology are the rapid deposition of ash at all sites, i.e. instantaneous in geological terms, and that the stratigraphic position of the ash in a sequence directly relates to the timing of the volcanic eruption. Processes that either delay the transportation of ash particles to a site or rework the material following initial deposition can have major impacts on the integrity of deposits as well-resolved isochronous markers. The operation of such processes has been investigated in many sedimentary environments (e.g. Ruddiman and Glover, 1972; Austin et al., 2004; Davies et al., 2007; Brendryen et al., 2010; Payne and Gehrels, 2010; Pouget et al., 2014; Todd et al., 2014; Watson et al., 2015) and are particularly crucial for cryptotephras, due to the absence of any visible stratigraphic features that would identify the position of the isochron and hence the timing of deposition and draw attention to any post-depositional reworking (Davies, 2015). For the marine environment it is critical to consider these processes due to its dynamic nature and the wide range of potential influences, especially when investigating sediments from glacial periods and high-latitude settings where ice-rafting processes could be a significant complicating factor.

Isochronous tephra deposits are formed in the marine environment if primary tephra fallout is deposited on the ocean surface, rapidly transported through the water column, deposited on the seabed and then preserved in the sediment by subsequent marine sedimentation (Figure 1). However, deposition onto other surfaces, e.g. ice sheets and sea-ice, subsequent rafting, and post-depositional reworking and redistribution processes, such as bioturbation and sedimentary loading, can have a major impact on the integrity of tephra deposits in this environment (Figure 1). For instance, these processes can affect the stratigraphic position of a tephra, a pertinent issue for marine sequences due to their lower resolution relative to other records, and potentially compromise the use of the deposit as an isochron. As such, it is essential that a full assessment of the sedimentation and depositional processes influencing the preservation, form and isochronous nature of marine cryptotephra deposits is undertaken. This is especially important if tephra horizons are to be used as tie lines to assess the relative timing of climatic changes between depositional environments.

Here we present an optimised protocol for marine cryptotephra studies. Our examples are derived from a range of depositional settings in the North Atlantic region (Figure 2), but the methodological approach could be applicable to many other marine settings. Within our approach, cryptotephras are identified and characterised using density separation, magnetic separation and electron probe micro-analysis (EPMA) techniques. We then employ a series of indicators to assess the isochronous nature of tephra deposits in the North Atlantic. These include (i) high-resolution shard concentration profiles, (ii) glass shard size variations, (iii) comprehensive single-shard geochemical analysis, and (iv) when available co-variance with ice-rafted debris (IRD). This work builds on previous studies, such as, Austin et al. (2004), Brendryen et al. (2010), Abbott et al. (2011, 2013, 2014, 2016), Davies et al. (2014) and Griggs et al. (2014), who used similar indicators to assess visible or cryptotephra deposits within single core sequences.

We advance that work, with a focus on the time-period between 25-60 ka BP in the North Atlantic, and define several key types of tephra deposit that share characteristics which are interpreted as being indicative of common transport, depositional and post-depositional processes. The tephra deposit types provide a basis for assessing the dominant controls on tephra deposition in different areas and time periods. Given the wide core network employed in this study we pinpoint sectors of the North Atlantic Ocean that preferentially preserve isochronous deposits and these underpin a marine tephra framework presented in Abbott et al. (submitted). These horizons are the most valuable for establishing independent high-precision correlations to the Greenland ice-core records to assess the relative timing of abrupt climate changes.

2. Methodology

2.1 Core Network

Thirteen marine sequences are included in our core network and each record was investigated using the same methodological approach (Figures 2 and 3; Table 1). Cores with well-developed proxy records were prioritised due to the overarching goal of assessing the relative timing of abrupt climate changes during the last glacial period. In addition, cores from areas with high sedimentation rates and sufficient material for contiguous tephra sampling were selected. Overall the network has a wide geographical spread, however, in some instances paired cores from nearly locations were investigated to assess the stratigraphic integrity of individual tephra deposits. It was not always possible to fulfil all of these requirements. For instance, contiguous samples were not available from MD95-2024 and a couple of sites, M23485-1 and GIK23415-9, do not have well-resolved records of abrupt climate changes. These sites were included, however, to increase the geographical extent and capture a wide range of depositional settings.

2.2 Identification of Cryptotephra Deposits

Cryptotephras were identified and characterised according to the methodological protocol outlined in Figure 3. Although most aspects of this marine-focussed methodological approach have been described separately in previous studies, here we synthesise the full procedure. Core sequences were initially analysed at a low-resolution (5 or 10 cm) using contiguous samples, i.e. samples taken along the whole length of depth intervals with no gaps between samples, to provide an initial quantified assessment of tephra content for the whole period of interest. Selected intervals were then reanalysed at a high-resolution (1 cm) depending on a range of factors, outlined in Section 3, consistent with other studies of both marine and terrestrial sequences (e.g. Pilcher and Hall, 1992; Lane et al., 2015; Matthews et al., 2015). Both low and high-resolution samples were processed according to the workflow outlined in Figure 3.

Within the protocol, samples are sieved to isolate glass tephra shards in three recommended size fractions (>125 µm, 80-125 µm and 25-80 µm). This is a development of prior studies that focused on coarser grain size fractions (e.g. >150 µm - Austin et al., 2004, Voelker and Haflidason, 2015; 63-125 µm and 125-150 µm – Brendryen et al., 2010), most typically utilised in the identification of foraminifera, and was driven by the increased identification of cryptotephras as fine-grained deposits in distal sequences (Davies, 2015). The smallest grain-size fraction (25-80 µm) was split using heavy liquid separation into density fractions most likely to contain glass shards, a procedure initially developed to identify cryptotephras in terrestrial sediments (Turney, 1998; Blockley et al., 2005). Magnetic separation is an additional step utilised to separate paramagnetic basaltic material from minerogenic material with a similar high density (>2.5g/cm^3; Griggs et al., 2014). Whilst this technique is infrequently employed for terrestrial sequences, e.g. Mackie et al. (2002), it is routinely applied in this investigation to aid the isolation and identification of basaltic material. The high number and proportion of basaltic horizons, relative to rhyolitic horizons, identified in this study demonstrates the value of including this technique within marine cryptotephra studies in the North Atlantic. During low-resolution analysis magnetic separation was only utilised on the 25-80 µm size fraction, because the time required for this process was longer than the time required to count shards from an unseparated sample of the larger fractions. However, during preparation of samples for geochemical analysis these larger fractions were magnetically separated alongside the 25-80 μm fraction to provide a purer basaltic glass sample.

If a low-resolution tephrostratigraphy was being constructed all fractions were inspected for tephra content using optical microscopy (i.e. >125 μm, 80-125 μm, 2.3-2.5 g/cm^3 and the >2.5 g/cm^3 magnetic fraction; step 12). However, when tephra concentration profiles were refined at a higher 1 cm resolution some fractions were not inspected. For example, if no rhyolitic material was present at a low resolution the 2.3-2.5 g/cm^3 fraction was not inspected.

Depending on the nature of the samples and the tephra contained within a sequence, alternative or additional steps were occasionally adopted (Figure 3). For instance, in some cores sediment clusters, that appear to consist of sediment bound together by biogenic silica, were observed (see also Ponomareva et al., in press). These clusters were broken down using a weak treatment of sodium hydroxide (NaOH) (step 5). This chemical treatment could also be undertaken after step 3 if clusters are known to be present following initial investigations. In such a case, the HCl should be washed out of the sediments, but no re-sieving is necessary. NaOH has previously been used in cryptotephra studies to remove biogenic silicates (e.g. Rose et al., 1996), with samples warmed to 90°C for 4 hours, however, it was found that treatment at room temperature for 1 hr was sufficient to disaggregate the sediment clusters in this study. As a precaution NaOH treatment was avoided when samples were being prepared for geochemical analysis, as it has been suggested that NaOH could cause geochemical modification (e.g. Blockley et al., 2005). However, other studies have shown that such treatments do not affect the glass composition (e.g. Steinhauser and Bichler, 2008) and experimentation by Ponomareva et al. (in press) indicates that electron-probe micro analysis (EPMA) analyses are unaffected by this weak NaOH treatment.

To quantify exceptionally high shard concentrations (~>10,000 per 0.5 g dry weight sediment (dws)) samples were spiked with Lycopodium spore tablets containing a known quantity of pollen grains (step 10). The ratio between glass shards and pollen grains is then used to quantify shard concentrations (e.g. Griggs et al., 2014). This is an adaption of a standard pollen counting approach previously applied to tephra studies by Gehrels et al. (2006). Typically, it is not known if this quantification approach is required until low-resolution analysis has been conducted. As such, if high shard concentrations were observed in low-resolution samples and it became apparent that shard concentrations would exceed 10,000 shards, counting was halted and the additional step of spiking samples was incorporated into high resolution analysis of those sections.

2.3 Geochemical Analysis of Cryptotephra Deposits

Shard concentration profiles are employed to select samples for geochemical analysis using the criteria outlined in Section 3. Samples were re-processed using steps 1-9 of the procedure, however, the fractions of interest were then mounted in epoxy resin on 28 × 48 mm microprobe slides to permit thin section preparation (Figure 3). When high shard concentrations were present all material from the fraction was mounted directly on to the slides. When tephra was only present at a low concentration (~<50 per 0.5 g dws) glass shards were picked onto a microprobe slide using a micromanipulator. Shards prepared by this method are easier to locate during sectioning and EPMA analysis. Flat and polished thin sections of the individual glass shards were produced for EPMA analysis using decreasing grades of silicon carbide paper and 9, 6 and 1 μm diamond suspension.

EPMA was conducted at the Tephra Analytical Unit, University of Edinburgh using a Cameca SX100 with five wavelength dispersive spectrometers over a number of analytical periods. All shards were analysed using the same operating conditions outlined in Hayward (2012). Pure metals, synthetic oxides and silicate standards were used for calibration. The secondary standards of Cannetto Lami Lava, Lipari and BCR2g were analysed at regular intervals to monitor for instrumental drift within analytical sessions, to assess the precision and accuracy of analysed samples and to provide a cross-check of the comparability of analyses between analytical periods. A large number of shards (~20-40 individual shards) were analysed for each deposit to provide comprehensive characterisations that underpin the assessment of taphonomic processes, depositional controls and the isochronous nature of deposits. For all analysis and data comparison the major element data were normalised to an anhydrous basis, i.e. 100 % total oxides, however, the raw geochemical data utilised here are provided in the Supplementary Data alongside secondary standard analyses.

3. Constructing a Tephrostratigraphy

The two major indicators that we employ to assess the integrity of marine tephra deposits are (i) contiguous high-resolution shard concentration profiles and (ii) rigorous geochemical characterisation of the glass tephra shards. These are the key aspects of the tephrostratigraphies defined in this work. Constructing a tephrostratigraphy, however, involves a series of selections and we illustrate our approach, which aimed for consistency and comparability between cores, with reference to the record of brown (basaltic) shards in the MD99-2251 core from the Iceland Basin between 1650-1950 cm depth (Figure 4). There was a distinct lack of colourless shards in this core section but a slight increase was observed towards the base, which can be related to reworking and redistribution of the underlying North Atlantic Ash Zone II (NAAZ) II (see Section 4).

First a low-resolution shard concentration profile is constructed to determine the overall presence of tephra and to define the background level of glass shards within a sequence (e.g. Figure 4a). All notable shard peaks were then re-analysed at a high-resolution (1 cm) to refine their stratigraphic position. This step is crucial as the peak in concentration is typically thought to represent the timing of atmospheric fallout from a volcanic event (e.g. Ruddiman and Glover, 1972; Jennings et al., 2002; Davies et al., 2012). Theoretically it is possible for the maximum shard concentration peak to lie below the original depth of deposition, based on an interplay of the extent of mixing within and depth of the mixing layer and the sedimentation rate at the site, however, the impact of this has been assessed as negligible in practice (Berger and Heath, 1968; Ruddiman and Glover, 1972). Indeed, our focus on high sedimentation rate sites would negate this effect, however, it is recommended that this is considered for individual horizons if they are to be used as isochronous tie-lines between sequences.

Selecting which peaks to refine at a 1 cm resolution depends on the peak versus background concentrations, the shape and discreteness of peaks and replication across grain-size fractions (e.g. Figure 4a). To some extent there is subjectivity in the selection of peaks and no consistent concentration thresholds could be defined due to variability in peak and background shard concentrations both within and between the core sequences. In most instances, but not exclusively, shard concentrations in the 25-80 μm fraction displayed the greatest variability and presence within the records and were the prime criteria for these selections (e.g. Figure 4a). For some cores, high-resolution investigations were extended over intervals wider than the main peaks to provide a greater constraint on shard concentration variations (e.g. between 1678-1698 cm in MD99-2251; Figure 4a) and/or additional samples were analysed to determine if smaller peaks were due to increased input of material from a volcanic event or general fluctuations in background shard concentrations (e.g. between 1869-1874 cm and 1879-1884 cm in MD99-2251; Figure 4a). In addition, the time required for processing and analysing the number of selected samples was considered.

Reanalysing selected sections at a high-resolution allows an integrated shard concentration profile to be constructed (e.g. Figure 4b) that, in general, constrains the shard peaks to 1 or 2 cm and higher concentrations were normally observed in the high-resolution counts (e.g. peaks at 1680-1681 cm and 1904-1905 cm depth in MD99-2251; Figure 4b). This observation was anticipated, as the low-resolution counts should provide an average of the tephra concentration over the sampling interval, and has been observed for other cores within the network. However, there are some examples where lower peak concentrations or very few shards were observed in the high-resolution samples (e.g. the 1869-1874 and 1879-1884 cm sections in MD99-2251; Figure 4b). This may be due to uneven lateral distribution of tephra shards within core sequences, a lack of horizontal continuity and tephra shards being constrained in pods or lenses. Tephra distributions of this nature have been observed in thin section (2D) and X-ray microtomography (3D) analysis of North Atlantic marine tephra sediments (Griggs et al., 2014, 2015). These additional methods can provide further sedimentological information to aid isochron placement and the interpretation of post-depositional processes, however, at present they have not been widely applied to tephra deposits in our network.

Once an integrated tephrostratigraphy is defined shard peaks are selected for geochemical analysis to allow the assessment of volcanic source and deposit integrity. Peaks were selected using criteria akin to those used to pinpoint samples for high-resolution analysis, i.e., discreteness relative to background concentrations, replication across grain-size fractions and processing and analysis time (e.g. Figure 4b).

4. Results

4.1 Classification of individual tephra deposits

We applied the same approach to construct a tephrostratigraphic record for all cores within our network and tephra deposits were identified in the vast majority of records. Tephra shard concentration profiles, geochemical characterisations and other indicators, such as shard size and co-variance with IRD, were integrated for these tephra deposits to define a deposit type classification scheme (Table 2). Five deposit types that share similar physical characteristics reflecting common modes of delivery and post-depositional reworking are identified (Table 2). This classification scheme is mainly based on deposits of brown glass shards (i.e. basaltic material) due to the relative lack of colourless shard deposits. However, Type 3, is an exception and is based on deposits that are most commonly associated with colourless shards related to NAAZ II, the most widespread silicic tephra found within our core network.

Deposit Types 1,2 and 3 are all characterised by distinct concentration peaks, however, their profiles vary in form, displaying discrete (e.g. Figure 5ai), bell-shaped (e.g. Figure 6ai) and asymmetric (e.g. Figure 7ai) forms respectively, and in spread ranging from 1 cm to up to

100 cm (Table 2). These contrasting features are attributed to variable shard concentrations between the deposit types and differential influence of post-depositional reworking. For instance, the low shard concentrations in Type 1 deposits contributes towards their discreteness. Whilst this may result from limited post-depositional reworking, it is also possible that the low concentration of tephra deposited at the sea-bed is not an adequate tracer of such activity. Reworking such as bioturbation, however, would most likely not impact the isochron position (see Section 3). In contrast, the higher input concentrations associated with Type 2 deposits allows the tephra shards to act as a tracer for bioturbation (e.g. Ruddiman and Glover, 1972; Griggs et al., 2015), which creates the upward and downward tails in deposition and roughly bell-shaped profile. This has often been viewed as the classic form of tephra deposits preserved in marine records (e.g. Ruddiman and Glover, 1972).

For Type 3 deposits the extremely high shard concentrations rapidly isolated underlying sediment from bioturbative activity and restricted downward migration of shards, as observed for the FMAZ II deposit in Griggs et al. (2015). The upward tail and continued deposition of tephra is primarily attributed to secondary deposition of glass shards from the same volcanic event from the surrounding sea-bed due to bottom current transportation. Bioturbative reworking may have also contributed towards increasing the overall spread of these deposits. In combination these two factors create the observed asymmetric profile (e.g. Figure 7ai; Table 2). Additional samples in the overall declining concentration profile of Type 3 deposits were sometimes analysed, particularly when subsidiary peaks were observed, in case any subsequent volcanic events were obscured within the upward tail. In all instances these additional analyses had an identical composition to shards in the main peak, corroborating the assertion that the upward tail was formed mainly through reworking of material from a single eruption (e.g. Figure 7ai).

Deposit Types 1,2 and 3 are most likely derived from single depositional events, yet their isochronous nature can only be fully determined by assessing the relative homo/heterogeneity of their geochemical signature. Type 1 and 3 deposits have a homogenous signature, i.e. all analysed shards form a single geochemical population most likely sourced from one volcanic eruption, which strongly suggest that they were deposited via primary airfall and are useful isochronous tephra markers (e.g. Figure 5aii for Type 1 deposits and Figure 7ai for a Type 3 deposit). Type 2 deposits are sub-divided into Type 2A, which have a homogenous composition, and Type 2B, which have a heterogenous composition, i.e. the analysed shards form multiple populations and/or reveal a widespread of analyses with high variability and limited consistency. Figures 6a and 6b provide examples of homogeneity for two Type 2A deposits, whilst, Figure 5b provides examples of the heterogeneity observed for two Type 2B deposits. This sub-categorisation is important as the homogenous Type 2A deposits are likely to be isochronous, akin to Type 1 and 3 deposits, while the heterogeneity of Type 2B deposits most likely reflects the deposition of products from multiple eruptions and probably secondary transport processes that affect the isochronous nature of the horizons. For example, geochemical heterogeneity is a key indicator of transport via iceberg rafting and the amalgamation of the products of closely timed eruptions (Griggs et al., 2014). An additional line of evidence for Type 2B deposits is co-variance of shard concentrations with IRD records. The relative proportion of shards across the different grain-size fractions can also help determine transport processes as sea-ice rafting typically transports shards larger than would be expected via primary airfall to distal sites (e.g. Austin et al., 2004). Overall, for Type 2 deposits a careful assessment of a range of key indicators is required to determine their value as isochronous deposits.

In contrast, to the single concentration peaks displayed by deposit Types 1,2 and 3, Type 4 deposits display multiple peaks over a period of elevated shard concentrations whereas Type 5 deposits are characterised by tephra in multiple consecutive samples, but no clear pattern or peaks in shard concentrations (Table 2). In most cases, the multiple peaks seen in the Type 4 deposits display heterogeneous compositions but typically a common geochemical signature, e.g. the wide 456-473 cm depth deposit in MD04-2820CQ (Figure 7b; Abbott et al., 2016). This indicates that the entire deposit is an amalgamation of eruptive material from several, closely timed, volcanic eruptions and that the multiple peaks are the product of secondary transport processes (e.g. bioturbation and bottom current reworking) rather than primary airfall. Alternatively, the glass shards found in Type 4 deposits may have been amalgamated during deposition on the Icelandic ice-sheet and subsequently transported to core sites via iceberg rafting. As with Type 2B deposits, further insights into the mode of deposition may be gained by comparing shard concentration profiles with iceberg rafting proxies. Without a distinct concentration peak or geochemical evidence that they were sourced from a single eruption Type 4 deposits typically cannot be utilised as isochronous marker horizons for high-precision correlations. However, they have the potential to be used as regional marine-marine core tie-lines, as suggested for FMAZ III by Abbott et al. (2016).

Type 5 deposits are commonly identified during low-resolution investigations. Only selected deposits were re-evaluated at a high-resolution and for geochemical composition. No distinct concentration peaks were identified, and geochemical analyses revealed heterogenous populations of shards that were geochemically identical to underlying deposits, e.g. NAAZ II. As such, Type 5 deposits are interpreted as a background of glass shards that are deposited at the core sites and dispersed in the sediment column by remobilisation and reworking processes. These background signals vary between sites and may mask and hamper the identification of primary airfall events that only deposited a low concentration of glass shards. High-resolution analysis coupled with intensive geochemical characterisation may isolate such events and would be appropriate if specific volcanic events were being targeted, however, this was not feasible within our extensive core network.

4.2 Categorising core sequences using the tephra classification scheme

The tephra classification scheme has been employed to categorise the cores according to the presence and dominance of different deposit types. Four core categories have been identified (Figure 8) and range from sites dominated by primary airfall deposits (green sites) to sites with deposits affected by secondary processes (red sites). In addition, very few shards were identified in the northernmost (JM04-25PC from the Western Svalbard slope) and southernmost (MD01-2444 from the Iberian Margin) records. Trace amounts (1-2 shards) were identified in some low-resolution samples but none were replicated as significant deposits during high-resolution analysis.

4.2.1 Core dominated by Type 1 deposits

Only two marine sequences exclusively contain Type 1 deposits, MD04-2822 from the Rockall Trough and MD04-2829CQ from the Rosemary Bank (Figure 8). The Type 1 deposits are discrete peaks in brown shard concentrations constrained within ~1 cm and both sites have a limited background of brown shards over the period of interest (e.g. Figure 5ai). Shards from the discrete peaks have single homogenous geochemical populations that can be directly related to single volcanic source regions (Figure 5aii) and as such are thought to represent isochronous marker horizons. The shard concentrations were low (~5-40 shards per

0.5 g dws in the 25-80 µm fraction) and occasionally replicating these peaks to extract shards for geochemical analysis was challenging. This may be a consequence of the uneven distribution of shards within the cores, however, the successful identification of these Type 1 deposits does demonstrate how the approach adopted in this work can be used to trace such low concentration deposits.

4.2.2 Cores containing Single Type 2A Deposits

Two cores, MD95-2010, from the Norwegian Sea, and MD01-2461, from the Porcupine Seabight, each contain just one significant tephra deposit with bell-shaped shard concentration profiles (Figure 6ai and bi). These deposits were identified because a significant number of shards were isolated over 10-20 cm intervals in the low-resolution counts. Given their homogenous geochemical compositions, these are both classified as Type 2A deposits (Figure 6aii and bii) and are thought to be isochronous markers. Evidence of upward reworking within MD01-2461 is seen by a small subsidiary tephra shard peak positioned 4-5 cm above the highest shard concentrations with an identical geochemical composition at both depths (Figure 6b). In both cores only trace amounts (<2-3) of shards were present in the rest of the low-resolution samples, apart from ~10 shards identified around NAAZ II in MD95-2010.

4.2.3 Cores containing Mixed Deposit Types

Five of the core sites have been grouped into this category (Figure 8) and contain a range of deposit types. Type 2 deposits dominate and these are typically relatively discrete with high shard concentrations, however the geochemical compositions range between homogenous

(Type 2A) and heterogenous (Type 2B). Type 4 deposits are also present in some sequences and at most sites the rhyolitic component of NAAZ II is present as a Type 3 deposit. The MD04-2820CQ record is a prime example of this category. It contains a number of Type 2 deposits, with differing geochemical homogeneity, the FMAZ III as a Type 4 deposit and the NAAZ II rhyolitic component as a Type 3 deposit (Abbott et al., 2016). The variability in tephra deposit types means that a careful assessment of deposits is required and strongly suggests that the depositional controls at these sites varied temporally throughout the last glacial period.

4.2.4 Core dominated by Type 2B and Type 4 deposits

Two cores have been grouped within this category, SU90-24 from the Irminger Basin and M23485-1 from the Iceland Sea (Figure 8). These sites are characterised by multiple concentration peaks within a high background level of shards, e.g. 1,000-10,000s of shards per 0.5 g dws. Peaks in shard concentration are not well-resolved in these records and the distinct contrast between SU90-24 and a Type 1 dominated core (MD04-2822) is shown in Figure 5. For SU90-24, single-shard analyses from some of the concentration peaks have highly heterogenous geochemical signatures, with a wide range of major oxide values that span several different Icelandic volcanic systems (Figure 5b). Given the shard concentration profiles and compositional results, these deposits are classified as Type 2B and Type 4. M23485-1 is dominated by Type 4 deposits with two major depositional pulses of heterogenous basaltic and rhyolitic material. Overall, the deposits found in these cores cannot be considered as isochronous horizons.

5. Discussion - Controls on Ash Deposition and Preservation

The core categorisation highlights that a diverse range of tephrostratigraphies were preserved during the last glacial period across the North Atlantic. Geographical clustering of similar core sites suggests that there were both spatial and temporal controls on ash deposition. Various factors could have controlled the transport and deposition of tephra, including (i) the nature of volcanism inputting tephra into the system, (ii) atmospheric dispersal patterns and distance from eruptive source, (iii) rafting by icebergs and sea-ice and (iv) the rate and nature of sedimentation. Local factors may have also operated at individual cores sites. Through an assessment of these factors we propose that for our core categories we identify common controls operating within different sectors of the North Atlantic (Figure 9).

5.1 Frequency and Composition of Icelandic Volcanism

The marine tephra records are ultimately controlled by the nature and frequency of Icelandic eruptions as this provides the primary input of tephra into the North Atlantic. Currently the most well-resolved record of Icelandic eruptions during the glacial period is derived from the Greenland ice-cores (Bourne et al., 2015) as proximal records are relatively limited due to the removal of material by glacial activity and the burial of deposits by subsequent volcanic activity. Within the Greenland ice-cores over 99 tephra deposits have been identified in this time period, which is significantly higher than the number identified within our marine tephra framework, but could suggest that some of the marine deposits have amalgamated material from multiple eruptions (e.g. FMAZ III in JM11-19PC and MD04-2820CQ; see Figure 7b). Within our core network there is a greater abundance of basaltic horizons in comparison to rhyolitic deposits, which is consistent with the Greenland ice-core records, as 95 % of these deposits are basaltic (Bourne et al., 2015). This dominance of far-travelled basaltic material within distal sites could be due to the increased ice cover during the last glacial period which implies that the horizons were derived from subglacial phreatomagmatic eruptions, which can enhance the explosivity of basaltic eruptions due to the presence of water (Larsen and Eiríksson, 2008). The relative lack of rhyolitic horizons in the ice-cores suggests that the rhyolitic background of shards observed in many of the marine records is most likely due to reworking of material from NAAZ II, rather than resulting from subsequent volcanic activity.

5.2 Atmospheric Dispersal Patterns and Proximity to Iceland

Following a volcanic eruption the wind-driven dispersal patterns will dictate the location of airfall deposition. The proximity of a core site to the volcano is important as the grain-size, shard concentration and thickness of airfall deposits decreases exponentially away from the eruptive source. Atmospheric transport skews this relationship with extended transport of material along transport axes downwind from the eruptive source and this bias is more evident at distal sites (Sparks et al., 1981; Pyle, 1989; Lacasse, 2001).

The four cores solely preserving deposits thought to be transported via primary airfall (i.e. green and orange sites containing Type 1 and Type 2A deposits: MD95-2010, MD04-2829CQ, MD04-2822 and MD01-2461) are located between the south and east of Iceland, in an oceanic sector stretching from the south coast of Ireland to the west coast of Norway, with the two green sites containing multiple deposits lying close together towards the SE off the west coast of Scotland (Figure 9). Other sites that preserve a mix of deposit types including some deposited via atmospheric transport, i.e. yellow coded sites, also generally lie to the south and east of Iceland with the exception of MD95-2024 (Figure 9). This clustering of sites suggests that tephra was transported from Iceland via westerly winds, consistent with dominant wind patterns and the nature of Icelandic eruptions.

Modern observations indicate that wind direction changes progressively with altitude in the troposphere, with easterlies dominating at ground level shifting to southerly at a low level (1.4 km) and westerlies in the upper troposphere and lower stratosphere between 9-15 km throughout the year (Lacasse, 2001). Above 15 km altitude seasonal variability is observed with strong westerlies during the autumn and winter and relatively weak easterlies during the spring and summer (Lacasse, 2001). The modern atmospheric patterns are utilised as an analogue for dispersal of tephra during the glacial period as the reconstruction of glacial wind patterns is complex. Studies do suggest, however, that surface circulation was more intense over the North Atlantic during the last glacial period (e.g. Mayewski et al., 1994; Kutzbach and Wright, 1985). Plume heights from modern basaltic eruptions similar in nature to those that occurred during the last glacial period (e.g. Vatnajökull 1996, Hekla 2000, Grímsvötn 2004 and 2011 and Eyjafjallajökull 2010) were typically between ~8-15 km with some reaching 25 km altitude (Gudmundsson et al., 2004; Höskuldsson et al., 2007; Kaminski et al., 2011; Oddsson et al., 2012; Petersen et al., 2012). For older eruptions, Lacasse (2001) deduced from proximal and distal grain sizes that the Saksunarvatn Ash, erupted from Grímsvötn in the early Holocene, produced an eruption column of at least 15 km. Eruptive plume heights together with dominant wind directions suggest that basaltic tephra was mainly atmospherically transported away from Iceland in an easterly direction and is consistent with our findings.

Southward atmospheric dispersal of some tephras, to core sites such as MD99-2251 and MD04-2820CQ, may be a consequence of modification by more variable surface wind conditions that reflect the weather at the time of an eruption (Lacasse, 2001). A similar scenario was observed for the Eyjafjallajökull 2010 eruption, with weather conditions exerting a strong influence following initial easterly transport of tephra (Davies et al., 2010). Other variable influences such as precipitation, the timing of the eruption, style of volcanism, magma discharge rate and height of eruptive column may have also created differences from the general pattern for individual eruptions. Although our observations indicate dispersal towards the south, no tephra deposits were preserved in the southernmost site MD01-2444, most likely due to the long distance between this site and the main Icelandic source.

Preferential atmospheric transport of ash to the east and south of Iceland is also consistent with the identification of airfall tephra horizons from Iceland in terrestrial deposits from sites in NW Europe (e.g. Lawson et al., 2012) and their absence to the west and southwest of Iceland (e.g. Greenland – Blockley et al., 2015; eastern North America - Pyne-O'Donnell et al., 2012; Mackay et al., 2016). Tephra is preserved at the most westerly site, MD95-2024. This core is downwind and the second furthest from Iceland with greater peak and background shard concentrations relative to closer downwind sites such as MD04-2829CQ and MD04-2822. This conflicts with the expected atmospheric dispersal pattern of tephra and proximity to source, strongly indicating that other processes were controlling tephra delivery to the North Atlantic west of Iceland.

The observation of limited atmospheric dispersal in a northerly direction from Iceland has some conflicts with the observations of Bourne et al. (2015) who inferred direct transport of ash in a north westerly direction to the Greenland ice-sheet (Figure 9). However, this could be a consequence of marine sites north of Iceland being more dominantly influenced by other controls, such as ice-rafting deposition of tephra (see discussion below), which masked any isochronous deposits. The distance from source was highly likely to be a dominant control on the non-preservation of tephra at the most northerly site JM04-25PC.

Overall, therefore, while atmospheric transport was the primary mechanism delivering tephra to the green and orange sites it was only a partial control on the delivery of tephra to the yellow sites. At those locations other controls had an additional influence, leading to the identification of some non-isochronous deposits.

5.3 Ice-Rafting of Tephra and Ocean Currents

The potential for tephra to have been rafted either by sea-ice or icebergs prior to deposition in the glacial North Atlantic has been highlighted previously and this process can transport material along different trajectories and further from the source than atmospheric dispersal. Three distinct areas that preserve tephra deposited by rafting processes, i.e. Deposit Types 2B and 4, have been identified. These areas are the Iceland Sea and Irminger Basin to the north and west of Iceland (core sites M23485-1 and SU90-24), the mid Atlantic (MD95-2024, MD99-2251, GIK23415-9, MD04-2820CQ) and NE of the Faroe Islands (JM11-19PC). Whilst the Iceland Sea and Irminger Basin were heavily influenced by these processes throughout the 25-60 ka BP period, both Type 2A and Type 2B deposits were preserved in the other two areas suggesting that the influence of rafting was temporally variable (Figure 8).

Surface ocean currents have a huge role to play in the trajectory of tephra-bearing sea-ice and icebergs away from Iceland (Bigg et al., 1996) and thus the deposition of tephra at core sites during melting. Modern surface ocean currents are illustrated on Figure 9 and are used as an analogue for the glacial period. The North Atlantic Drift (NAD) from the SW dominates the warm surface ocean currents and splits into the Irminger Current south of Greenland and the North Iceland Irminger Current around Iceland before flowing into the Nordic Seas. Cold currents are dominated by the East Greenland Current flowing down the east coast of Greenland. A distinct feature of the surface circulation is the subpolar gyre, an anti-clockwise ocean surface circulation south of Iceland (Figure 9). These surface ocean currents would have strongly influenced ice-rafting but the source of icebergs and sea-ice extent was also an important factor.

The expanded size of the LGM ice-sheet over Iceland suggests that ice calving margins could have been located all around the island (Figure 9). With the majority of the major volcanic centres located in the south of the island, icebergs from the southward margin may have contained a greater concentration of tephra, however, local atmospheric transport north, east and west of the volcanoes would have contributed material to icebergs calving from all of these margins. The surface circulation patterns shown in Figure 9 suggests that icebergs from all margins could have been transported in surface ocean currents. Sea-ice reconstructions have shown that its extent over the North Atlantic region varied in time with the DO and Heinrich events (Hoff et al., 2016). It has been suggested that sea-ice retreated abruptly during the warming at the start of interstadials, but spread rapidly from the coast of Greenland during interstadial cooling with perennial sea-ice extending beyond Iceland during cold stadials and reaching a greater extent during Heinrich events (Figure 9; Hoff et al., 2016). This temporal variability in sea-ice coverage and its rafting along similar trajectories to those proposed for icebergs is likely to have played a role in the dispersal of tephra.

Iceberg rafting from the north coast of Iceland was the likely primary control on tephra deposition north and west of Iceland. The M23485-1 site lies close to the northern margin of the LGM Icelandic ice sheet and icebergs calved from this margin could have been entrained within the East Greenland Current and deposited material over the SU90-24 site. In addition, sea-ice rafting may have contributed towards this pattern of tephra deposition as the latter site lies within the stadial perennial ice-sheet limits and would have been covered early in the advances during interstadial cooling phases. Within the mid-Atlantic area Icelandic icebergs transported in the sub-polar gyre are likely to have deposited material at both the MD95-2024 and MD99-2251 sites. The MD04-2820CQ and GIK23415-9 sites lie within the IRD Belt, an area of the North Atlantic within which IRD from the Laurentide Ice Sheet was deposited during Heinrich Events, and may have been influenced by Icelandic icebergs transported in this zone by surface currents (Figure 9). Indeed, glass shards have been found in association with the lithic Heinrich layers (e.g. Obrochta et al., 2014). The influence of sea-ice rafting in the mid-Atlantic would have been temporally variable throughout the glacial period and should not be ruled out as a potential process for ash transport and deposition as MD95-2024 and MD99-2251 lie close to the stadial perennial sea ice limit and MD04-2820CQ and GIK23415-9 lie close to the Heinrich event limit (Figure 9). The area to the NE of the Faroe Islands, the JM11-19PC site, may have been influenced by both rafting processes, with icebergs transported from the North coast of Iceland in the North Iceland Irminger Current and it lies close to the limit of perennial sea-ice during stadial periods. For all sites potentially affected by rafting processes key indicators such as the level of geochemical heterogeneity and shard sizes should be utilised to assess individual deposits.

The lack of rafted deposits in the MD04-2822 and MD04-2829CQ cores may be due to the Rockall Trough, the main pathway by which the warm North Atlantic surface water flows northward into the Norwegian Sea, effectively isolating them from the influence of Icelandic icebergs. The sites lie close to the stadial perennial sea ice limit so could be susceptible to sea ice rafting, however, the tephrostratigraphic records strongly indicate that this process has not deposited tephra at these particular sites. Continuous sea-ice cover can be ruled out as a potential control on the lack of tephra preservation at the northerly JM04-25PC site. The reconstructed sea-ice limits from Hoff et al. (2016) suggest that while the site is the most northerly sea-ice cover was limited to stadial phases and Heinrich events and was not greater than at other sites, e.g. SU90-24 and M23485-1, containing significant tephra deposits (Figure 9).

5.4 Nature and Rate of Sedimentation

Sedimentation rates are a further important a control on tephra preservation. They provide information on the nature of sedimentation and slower rates of sedimentation increase the likelihood that the products of separate but closely timed eruptions are amalgamated. Table 1 presents approximate average sedimentation rates for all the sites in the core network between 25-60 ka BP. In general, all the sites had relatively high sedimentation rates, a bias created by our prioritisation of sites to include in the network (see Section 2.1).

These high sedimentation rates may indicate that, in addition to sedimentation occurring through pelagic settling, bottom currents were also transporting material to the sites (Rebesco et al., 2014). Thus, the sites incorporated in the network may have an increased susceptibility to secondary deposition of tephra shards via bottom current reworking. This process could account for the persistent low background levels of glass shards at most sites (Type 5 deposits) and occasional outlying single shard analyses in the tephra deposits (see Abbott et al., submitted). However, bottom current reworking does not appear to have been a significant control on the nature of these tephra records. The only deposit type that we interpret as being formed and affected by this process is Type 3 and this can be attributed to the exceptionally high peak shard concentrations in comparison to the other deposit types (Table 2). Almost exclusively Type 3 deposits are associated with NAAZ II, a unique event that led to the input of a sufficient concentration of shards into the oceanic system to be reworked and act as a tracer for bottom current activity. As with bioturbation, the lack of evidence of reworking for other deposits does not definitively demonstrate that this process was not occurring, because the tephra concentrations could have been too low to act as an adequate tracer.

There is no clear difference in sedimentation rates between the cores containing only isochronous deposits (i.e. green and orange sites) and those dominated by heterogenous secondary deposits (i.e. red sites) with estimated rates of 14-20 cm/ka and 17-19 cm/ka respectively (Table 1; Figure 8). However, in general the sites containing a mix of deposit types (yellow sites; Figure 8) have lower sedimentation rates, between 9-11 cm/ka, apart from the MD95-2024 site which had a rate of 22 cm/ka (Table 1). This contrast in sedimentation rates is a general reflection of these cores deriving from the deepest sites in the network, away from terrestrial sediment sources and the higher sedimentation rates observed on continental shelves (Figure 9). The low sedimentation rates may have contributed towards the occurrence of Type 2B and Type 4 deposits at these sites due to the increased likelihood of eruptive products being amalgamated. With Icelandic basaltic tephra horizons in the Greenland ice-cores having an average recurrence interval of ~1 per 200 years during this period (Bourne et al., 2015) and 200 years being represented by ~2 cm depth at the yellow sites it is highly likely that closely spaced eruptions were mixed. The lower sedimentation rates would also have contributed to slower upward migration of the bioturbation mixing zone, promoting the amalgamation of deposits and elongation of the shard concentration profile for Type 2 deposits. Each deposit must be evaluated individually as these sites may also be heavily influenced by rafting processes, which can produce Type 2B deposits with geochemical heterogeneity. Overall, the lower sedimentation rates and thus temporal resolution at all these sites could account for the lower number of tephra horizons identified within the marine core network in comparison to the Greenland ice-core records (see Abbott et al., submitted for further discussion).

5.5 Local Site Conditions

Based on their proximity to Iceland, atmospheric dispersal patterns and tephra rafting in the North Atlantic one might expect MD95-2010 and MD01-2461 to both contain a number of tephra deposits. Both, however, only contained a single tephra deposit, the FMAZ IV and NAAZ II respectively, strongly suggesting another factor was limiting the deposition of tephra at these sites. Both sites lie close to the former limits of LGM ice sheets and are amongst the shallowest sites in the network (Figure 9; Table 1). Higher levels of terrigenous sediment deposition might have masked or diluted the tephra records at these sites, especially if the material was large and/or dense as the tephra concentrations presented in this work are referenced to overall sediment weight.

5.6 Summary

Overall, whilst only a small area of the North Atlantic was disposed to solely preserving isochronous Type 1 and Type 2A deposits, these primary deposits can also be preserved in a wide area to the east and south of Iceland due to atmospheric dispersal patterns. Only a small area to the north and west of Iceland does not preserve any isochronous deposits. We suggest that the most significant factor complicating the tephrostratigraphic records is the rafting of tephra within icebergs and sea-ice, which can be constrained spatially but also displays temporal variability, particularly at sites within the central North Atlantic. In addition, the high frequency of Icelandic volcanic eruptions during the period provides a constraint on tephra records as despite our focus on sites with high sedimentation rates they are potentially still too low to resolve individual events.

6. Conclusions

This work provides an integrated methodology for the identification of cryptotephras in North Atlantic marine records alongside a protocol for assessing the integrity of deposits and the influence of primary and secondary transport and depositional processes. This has been applied to a widespread network of cores from which five key tephra deposit types with common physical characteristics and depositional and transport histories have been defined. These range from valuable airfall deposited isochronous horizons, to geochemically heterogenous deposits with complex histories, to persistent background signals of ash deposition. While the variety of deposit types observed in the glacial North Atlantic reflects the complexity of processes controlling the transport, deposition and post-depositional reworking of tephra and may be unique to this setting, the methodological approach for identification could underpin investigations in other oceanic regions.

A regional analysis of the tephrostratigraphic records has shown that a range of different controls influenced tephra deposition and the deposit types preserved at different sites within the North Atlantic over the last glacial period. A key area to the southeast of Iceland was sheltered from any ice-rafting influence and only isochronous airfall deposits have been isolated in these records. However, primary deposits were also identified in a wide oceanic sector between the south and east of Iceland, which could be the focus of future studies to identify further isochronous horizons or to trace those identified within this work. The significance of the isochronous horizons in this work is discussed in Abbott et al. (submitted), which defines the framework of marine tephra horizons for the 25-60 ka BP period in the North Atlantic region.

Acknowledgements

This work was financially supported by the European Research Council (TRACE project) under the European Union's Seventh Framework Programme (FP7/2007-2013) / ERC grant agreement no. [259253]. PMA also acknowledges support from the European Research Council under the European Union's Horizon 2020 research and innovation programme (grant agreement No 656381). Thanks to William Austin, Henning Bauch, Mark Chapman, Frederique Eynaud, Ian Hall, Claude Hillaire-Marcel, Elisabeth Michel, Tine Rasmussen, Bjørg Risebrobakken, James Scourse, Mara Weinelt and the British Ocean Sediment Core Research Facility (BOSCORF) for providing samples or access to the marine cores utilised within this study. We would like to thank Dr Chris Hayward for his assistance with the use of the electron microprobe at the Tephrochronology Analytical Unit, University of Edinburgh. Thanks also to Gareth James, Gwydion Jones and Kathryn Lacey (Swansea University) for assistance with laboratory processing. This paper contributes to the EXTRAS project (EXTending TephRAS as a global geoscientific research tool stratigraphically, spatially, analytical, and temporally within the Quaternary), an INTAV-led project (International Focus

Group on Tephrochronology and Volcanism) within the Stratigraphy and Chronology Commission (SACCOM) of the International Union for Quaternary research (INQUA).

Figures Captions

Figure 1: Flow chart of the transportation and depositional processes that could have affected tephra within the glacial North Atlantic prior to preservation in marine sediments. Adapted from Griggs et al. (2014).

Figure 2: Network of North Atlantic marine cores studied within this work and ice-cores mentioned within the text.

Figure 3: Flow chart of the consistent methodology utilised to determine the tephra content of cores within the marine network and extract and prepare glass shards for geochemical analysis. NaOH = sodium hydroxide. SPT = sodium polytungstate.

Figure 4: Example of the construction of a tephrostratigraphy using the MD99-2251 core. (a) Low-resolution brown glass shard concentration profiles split into three grain-size fractions. Blue bars denote depth intervals reinvestigated at a 1 cm resolution. (b) Integrated high and low resolution brown shard counts for the MD99-2251 core. Shard counts have been truncated for clarity. Shard counts in the 1686-1687 cm sample (*) are 4991, 1862 and 507 shards per 0.5 g dws in the 25-80, 80-125 and >125 µm grain-size fractions respectively. The shard count for the 25-80 µm grain-size fraction from the 1904-1905 cm sample (**) are 3776 shards per 0.5 g dws. Red bars denote samples depths from which glass shards were subsequently extracted for compositional characterisation.

Figure 5: Comparison of (i) tephrostratigraphic records and (ii) compositional characterisations of tephra deposits from the (a) MD04-2822 and (b) SU90-24 marine

sequences. Brown shard counts for the 25-80 μm grain-size fraction from 470-500 cm in SU90-24 have been truncated for clarity. Shard counts exceed 40,000 shards per 0.5 g dws, however, two peaks could be identified at 480-481 cm and 486-487 cm. Np(s) record for MD04-2822 from Hibbert et al. (2010). Magnetic susceptibility record for SU90-24 from Elliot et al. (2001). Geochemical fields for Icelandic volcanic systems from Bourne et al. (2015) and references within. Within MD04-2822 additional discrete peaks can be observed, e.g. at 1731-1732 cm and 1965-1966 cm, however, it was not possible to acquire sufficient material for geochemical characterisation.

Figure 6: Examples of shard concentration profiles and geochemical characterisations for Type 2A tephra deposits from two North Atlantic marine records within the network. (a) MD95-2010 (i) 910-920 cm high-resolution tephrostratigraphy of brown glass shards (ii) compositional variation diagrams of analyses from glass shards extracted from the 915-916 cm depth sample. Chemical classification and nomenclature for total alkalis versus silica plot after Le Maitre et al. (1989) and division line to separate alkaline and sub-alkaline material from MacDonald and Katsura (1964). Geochemical fields for Icelandic tholeiitic volcanic systems defined using whole rock analyses from Jakobsson et al. (2008) (Reykjanes), Höskuldsson et al. (2006) and Óladóttir et al. (2011) (Kverkfjöll) and Jakobsson (1979), Haflidason et al. (2000) and Óladóttir et al. (2011) (Grímsvötn and Veidivötn-Bardabunga). (b) MD01-2461 (i) 940-950 cm high-resolution tephrostratigraphy of colourless glass shards (ii) total alkalis versus silica plot of analyses from glass shards extracted from the 947-948 cm depth sample. Normalised compositional fields for the Icelandic rock suites derived from whole rock analyses in Jakobsson et al. (2008).

Figure 7: Examples of shard concentration profiles and geochemical characterisations for a (a) Type 3 and a (b) Type 4 deposits from two North Atlantic marine records within the network. (a) MD99-2251 (i) 1950-2030 cm tephrostratigraphy of colourless glass shards integrating low and high-resolution shard counts (ii) compositional variation diagrams comparing characterisations of colourless glass shards from 1974-1979 cm and 2014-2015 cm depth. (b) MD04-2820CQ (i) 450-480 cm high-resolution tephrostratigraphy of brown glass shards (ii) compositional variation diagrams comparing characterisations from four shard peaks within the Type 4 deposit. Data from Abbott et al. (2016). Chemical classification and nomenclature for total alkalis versus silica plot after Le Maitre et al. (1989) and division line to separate alkaline and sub-alkaline material from MacDonald and Katsura (1964).

Figure 8: Classification of core sites within the marine core network. See Section 4.2 for details of classes.

Figure 9: Primary controls and influences on the deposition of tephra within the glacial North Atlantic Ocean. Ocean surface currents and names from Voelker and Haflidason (2015) and Rasmussen et al. (2016). Currents: IC = Irminger Current; NIIC = North Iceland Irminger Current; EGC = East Greenland Current; EIC = East Iceland Current; NAD = North Atlantic Drift; SPG = Sub-polar Gyre. Last Glacial Maximum (LGM) ice limits from Dyke et al. (2002), Funder et al. (2011) and Hughes et al. (2016). Perennial sea ice limits from Hoff et al. (2016). Core classification from Figure 7.

Supplementary Information

Table S1: Major oxide concentrations of shards from tephra deposits in the MD04-2822 core. Deposits analysed are from the depths of (i) 1836-1837 cm (ii) 2004-2005 cm and (iii) 2017-2018 cm.

Table S2: Major oxide concentrations of shards from tephra deposits in the SU90-24 core. Deposits analysed are from the depths of (i) 340-342 cm (ii) 420-422 cm (iii) 480-481 cm and (iv) 486-487 cm.

Table S3: Major oxide concentrations of shards from the MD95-2010 915-916 cm tephra deposit.

Table S4: Major oxide concentrations of shards from MD01-2461 related to the rhyolitic component of North Atlantic Ash Zone II (II-RHY-1). Deposits analyses are at (i) 942-943 cm and (ii) 2014-2015 cm depth.

Table S5: Major oxide concentrations of shards from MD99-2251 related to the rhyolitic component of North Atlantic Ash Zone II (II-RHY-1). Deposits analyses are at (i) 1974-1975 cm and (ii) 947-948 cm depth.

Table S6a: Secondary standard analyses of the BCR2g standard made throughout analytical periods during which sample analyses presented in this work were analysed.

Table S6b: Secondary standard analyses of the Lipari standard made throughout analytical periods during which sample analyses presented in this work were analysed.

References

Abbott, P.M., Austin, W.E.N., Davies, S.M., Pearce, N.J.G., Hibbert, F.D., 2013. Cryptotephrochronology of a North East Atlantic marine sequence over Termination II, the Eemian and the last interglacial-glacial transition. Journal of Quaternary Science 28, 501-514.

Abbott, P.M., Austin, W.E.N., Davies, S.M., Pearce, N.J.G., Rasmussen, T.L., Wastegård, S., Brendryen, J., 2014. Re-evaluation and extension of the MIS 5 tephrostratigraphy of the Faroe Islands Region: the cryptotephras record. Palaeogeography, Palaeoclimatology, Palaeoecology 409, 153-168.

Abbott, P.M., Bourne, A.J., Purcell, C.S., Davies, S.M., Scourse, J.D., Pearce, N.J.G., 2016. Last Glacial Period Cryptotephra Events in an Eastern North Atlantic Ocean Marine Sequence: Exploring Linkages to the Greenland Ice-Cores. Quaternary Geochronology 31, 62-76.

Abbott, P.M., Davies, S.M., Austin, W.E.N., Pearce, N.J.G., Hibbert, F.D., 2011. Identification of cryptotephra horizons in a North East Atlantic marine record spanning marine isotope stages 4 and 5a (~60,000-82,000 a b2k). Quaternary International 246, 177-189.

Abbott, P.M., Griggs, A.J., Bourne, A.J., Chapman, M.R., Davies, S.M., submitted. Tracing marine cryptotephras in the North Atlantic during the Last Glacial Period: Improving the North Atlantic marine tephra framework. Submitted to Quaternary Science Reviews.

Austin, W.E.N., Wilson, L.J., Hunt, J.B., 2004. The age and chronostratigraphical significance of North Atlantic Ash Zone II. Journal of Quaternary Science 19, 137-146.

Berger, W., Heath, G.R., 1968. Vertical mixing in pelagic sediments. Journal of Marine Research 26, 135-143.

Bigg, G.R., Wadley, M.R., Stevens, D.P., Johnson, J.A., 1996. Prediction of iceberg trajectories for the North Atlantic and Arctic Oceans. Geophysical Research Letters 23, 3587-3590.

Blockley, S.P.E., Edwards, K.J., Schofield, J.E., Pyne-O'Donnell, S.D.F., Jensen, B.J.L., Matthews, I.P., Cook, G.T., Wallace, K.L., Froese, D., 2015. First evidence of cryptotephra in palaeoenvironmental records associated with Norse occupation sites in Greenland. Quaternary Geochronology 27, 145-157.

Blockley, S.P.E., Pyne-O'Donnell, S.D.F., Lowe, J.J., Matthews, I.P., Stone, A., Pollard, A.M., Turney, C.S.M., Molyneux, E.G., 2005. A new and less destructive laboratory procedure for the physical separation of distal glass tephra shards from sediments. Quaternary Science Reviews 24, 1952-1960.

Bourne, A.J., Cook, E., Abbott, P.M., Seierstad, I.K., Steffensen, J.P., Svensson, A., Fischer, H., Schupbach, S., Davies, S.M., 2015. A tephra lattice for Greenland and a reconstruction of volcanic events spanning 25-45 ka b2k. Quaternary Science Reviews 118, 122-141.

Brendryen, J., Haflidason, H., Sejrup, H.P., 2010. Norwegian Sea tephrostratigraphy of marine isotope stages 4 and 5: Prospects and problems for tephrochronology in the North Atlantic region. Quaternary Science Reviews 29, 847-864.

Davies, S.M., 2015. Cryptotephras: the revolution in correlation and precision dating. Journal of Quaternary Science 30, 114-130.

Davies, S.M., Abbott, P.M., Meara, Rh. H., Pearce, N.J.G., Austin, W.E.N., Chapman, M. R., Svensson, A., Bigler, M., Rasmussen, T.L., Rasmussen, S.O., Farmer, E.J., 2014. A North Atlantic tephrostratigraphical framework for 130-60 ka b2k: new tephra discoveries, marine-based correlations, and future challenges. Quaternary Science Reviews 106, 101-121.

Davies, S.M., Abbott, P.M., Pearce, N.J.P., Wastegård, S., Blockley, S.P.E., 2012. Integrating the INTIMATE records using tephrochronology: rising to the challenge. Quaternary Science Reviews 36, 11-27.

Davies, S.M., Elmquist, M., Bergman, J., Wohlfarth, B., Hammarlund, D., 2007. Cryptotephra sedimentation processes within two lacustrine sequences from west central Sweden. Holocene 17, 319-330.

Davies, S.M., Larsen, G., Wastegård, S., Turney, C.S.M., Hall, V.A., Coyle, L., Thordarson, T., 2010. Widespread dispersal of Icelandic tephra: how does the Eyjafjöll eruption of 2010 compare to past Icelandic events? Journal of Quaternary Science 25, 605-611.

Dokken, T.M., Jansen, E., 1999. Rapid changes in the mechanism of ocean convection during the last glacial period. Nature 401, 458-461.

Dyke, A.S., Andrews, J.T., Clark, P.U., England, J.H., Miller, G.H., Shaw, J., Veillette, J.J., 2002. The Laurentide and Innuitian ice sheets during the Last Glacial Maximum. Quaternary Science Reviews 21, 9-31.

Elliot, M., Labeyrie, L., Bond, G., Cortijo, E., Turon, J.-L., Tisnerat, N., Duplessy, J.-D., 1998. Millennial-scale iceberg discharges in the Irminger Basin during the last glacial period: Relationship with the Heinrich events and environmental settings. Paleoceanography 13, 433-446.

Elliot, M., Labeyrie, L., Dokken, T., Manthé, S., 2001. Coherent patterns of ice-rafted debris deposits in the Nordic regions during the last glacial (10-60 ka). Earth and Planetary Science Letters 194, 151-163.

Ezat, M.M., Rasmussen, T.L., Groeneveld, J., 2014. Persistent intermediate water warming during cold stadials in the southeastern Nordic seas during the past 65 k.y.. Geology 42, 663-666.

Funder, S., Kjeldsen, K.K., Kjær, K., Ó Cofaigh, C., 2011. The Greenland Ice Sheet during the past 30,000 years: a review. In Ehlers, J., Gibbard, P., Hughes, P.D. (eds) Quaternary Glaciations – Extent and Chronology: A Closer Look, pp. 699-714.

Gehrels, M.J., Lowe, D.J., Hazell, Z.J., Newnham, R.M., 2006. A continuous 5300-yr Holocene cryptotephrostratigraphic record from northern New Zealand and implications for tephrochronology and volcanic hazard assessment. Holocene 16, 173-187.

Griggs, A.J., Davies, S.M., Abbott, P.M., Coleman, M., Palmer, A.P., Rasmussen, T.L., Johnston, R., 2015. Visualising tephra sedimentation processes in the marine environment: the potential of X-ray microtomography. Geochemistry, Geophysics, Geosystems 16, doi: 10.1002/2015GC006073.

Griggs, A.J., Davies, S.M., Abbott, P.M., Rasmussen, T.L., Palmer, A.P., 2014. Optimising the use of marine tephrochronology in the North Atlantic: A detailed investigation of the Faroe Marine Ash Zones II, III and IV. Quaternary Science Reviews 106, 122-139.

Gudmundsson, M.T., Sigmundsson, F., Björnsson, H., Högnadóttir, T., 2004. The 1996 eruption at Gjálp, Vatnajökull ice cap, Iceland: efficiency of heat transfer, ice deformation and subglacial water pressure. Bulletin of Volcanology 66, 46-65.

Hall, I.R., Colmenero-Hidalgo, E., Zahn, R., Peck, V.L., Hemming, S.R., 2011. Centennial- to millennial-scale ice-ocean interactions in the subpolar northeast Atlantic 18-41 kyr ago. Paleoceanography 26, PA2224.

Hayward, C., 2012. High spatial resolution electron probe microanalysis of tephras and melt inclusions without beam-induced chemical modification. The Holocene 22, 119-125.

Hibbert, F.D., Austin, W.E.N., Leng, M.J., Gatliff, R.W., 2010. British Ice Sheet dynamics inferred from North Atlantic ice-rafted debris records spanning the last 175 000 years. Journal of Quaternary Science 25, 461-482.

Hoff, U., Rasmussen, T.L., Stein, R., Ezat, M.M., Fahl, K., 2016. Sea ice and millennial-scale climate variability in the Nordic seas 90 kyr ago to present. Nature Communications 7:12247.

Höskuldsson, Á., Óskarsson, N., Pedersen, R., Grönvold, K., Vogfjörð, K., Ólafsdóttir, R., 2007. The millennium eruption of Hekla in February 2000. Bulletin of Volcanology 70, 169-182.

Höskuldsson, Á., Sparks, R.S.J., Carroll, M.R., 2006. Constraints on the dynamics of subglacial basalt eruptions from geological and geochemical observations at Kverkfjöll, NE-Iceland. Bulletin of Volcanology 68, 689-701.

Hughes, A.L.C., Gyllencreutz, R., Lohne, Ø.S., Mangerud, J., Svendsen, J.I., 2016. The last Eurasian ice sheets – a chronological database and time-slice reconstruction, DATED-1. Boreas 45, 1-45.

Jakobsson, S.P., 1979. Petrology of recent basalts of the Eastern Volcanic Zone, Iceland. Acta Naturalia Islandia 26, 1-103.

Jakobsson, S.P., Jónasson, K., Sigurdsson, I.A., 2008. The three igneous rock suites of Iceland. Jökull 58, 117-138.

Jennings, A.E., Grönvold, K., Hilberman, R., Smith, M., Hald, M., 2002. High-resolution study of Icelandic tephras in the Kangerlussuaq Trough, southeast Greenland, during the last deglaciation. Journal of Quaternary Science 17, 747-757.

Jessen, S.P., Rasmussen, T.L., 2015. Sortable silt cycles in Svalbard slope sediments 74-0 ka. Journal of Quaternary Science 30, 743-753.

Kaminski, E., Tait, S., Ferrucci, F., Martet, M., Hirn, B., Husson, P., 2011. Estimation of ash injection in the atmosphere by basaltic volcanic plumes: The case of the Eyjafjallajökull 2010 eruption. Journal of Geophysical Research 116, B00C02.

Kutzbach, J.E., Wright Jr., H.E., 1985. Simulation of the climate of 18,000 years BP: Results for the North American/North Atlantic/European sector and comparison with the geologic record of North America. Quaternary Science Reviews 4, 147-187.

Lacasse, C., 2001. Influence of climate variability on the atmospheric transport of Icelandic tephra in the subpolar North Atlantic. Global and Planetary Change 29, 31-55.

Lane, C.S., Brauer, A., Martín-Puertas, C., Blockley, S.P.E., Smith, V.C., Tomlinson, E.L., 2015. The Late Quaternary tephrostratigraphy of annually laminated sediments from Meerfelder Maar, Germany. Quaternary Science Reviews 122, 192-206.

Larsen, G., Eiríksson, J., 2008. Holocene tephra archives and tephrochronology in Iceland – a brief overview. Jökull 58, 229-250.

Lawson, I.T., Swindles, G.T., Plunkett, G., Greenberg, D., 2012. The spatial distribution of Holocene cryptotephras in north-west Europe since 7 ka: implications for understanding ash fall events from Icelandic eruptions. Quaternary Science Reviews 41, 57-66.

Le Maitre, R.W., Bateman, P., Dudek, A., Keller, J., Lameyre, Le Bas, M.J., Sabine, P.A., Schmid, R., Sorensen, H., Streckeisen, A., Woolley, A.R., Zanettin, B., 1989. A Classification of Igneous Rocks and Glossary of Terms. Blackwell, Oxford.

Lowe, D.J., 2011. Tephrochronology and its application: A review. Quaternary Geochronology 6, 107-153.

MacDonald, G.A., Katsura, T. 1964. Chemical composition of Hawaiian lavas. Journal of Petrology 5, 83-133.

Mackay, H., Hughes, P.D.M., Jensen, B.J.L., Langdon, P., Pyne-O'Donnell, S.D.F., Plunkett, G., Froese, D.G., Coulter, S., Gardner, J.E., 2016. A mid to late Holocene cryptotephra framework from eastern North America. Quaternary Science Reviews 132, 101-113.

Mackie, E., Davies, S.M., Turney, C.S.M., Dobbyn, K., Lowe, J.J., 2002. The use of magnetic separation techniques to detect basaltic microtephra in glacial-interglacial transition (LGIT; 15-10 ka cal. BP) sediment sequences in Scotland. Scottish Journal of Geology 38, 21-30.

Martrat, B., Grimalt, J.O., Shackleton, N.J., de Abreu, L., Hutterli, M.A., Stocker, T.F., 2007. Four Climate Cycles of Recurring Deep and Surface Water Destabilizations on the Iberian Margin. Science 317, 502-507.

Matthews, I.P., Trincardi, F., Lowe, J.J., Bourne, A.J., Macleod, A., Abbott, P.M., Andersen, N., Asioli, A., Blockley, S.P.E., Lane, C.S., Oh, Y.A., Satow, C.S., Staff, R.A., Wulf, S., 2015. Developing a robust tephrochronological framework for Late Quaternary marine records in the Southern Adriatic Sea: new data from core station SA03-11. Quaternary Science Reviews 118, 84-104.

Mayewski, P.A., Meeker, L.D., Whitlow, S., Twickler, M.S., Morrison, M.C., Bloomfield, P., Bond, G.C., Alley, R.B., Gow, A.J., Grootes, P.M., Meese, D.A., Ram, M., Taylor, K.C., Wumkes, W., 1994. Changes in Atmospheric Circulation and Ocean Ice Cover over the North Atlantic During the last 41,000 Years. Science 263, 1747-1751.

Obrochta, S.P., Crowley, T.J., Channell, J.E.T., Hodell, D.A., Baker, P.A., Seki, A., Yokoyama, Y., 2014. Climate variability and ice-sheet dynamics during the last three glaciations. Earth and Planetary Science Letters 406, 198-212.

Oddson, B., Gudmundsson, M.T., Larsen, G., Karlsdóttir, S., 2012. Monitoring of the plume from the basaltic phreatomagmatic 2004 Grímsvötn eruption application of weather radar and comparison with plume models. Bulletin of Volcanology 74, 1395-1407.

Óladóttir, B.A., Sigmarsson, O., Larsen, G., Devidal, J.-L., 2011. Provenance of basaltic tephra from Vatnajökull volcanoes, Iceland, as determined by major- and trace-element analyses. The Holocene 21, 1037-1048.

Payne, R., Gehrels, M., 2010. The formation of tephra layers in peatlands: An experimental approach. Catena 81, 12-23.

Peck, V.L., Hall, I.R., Zahn, R., Elderfield, H., 2008. Millennial-scale surface and sub-surface paleothermometry from the northeast Atlantic, 55-8 ka BP. Paleoceanography 23, PA3221.

Peck, V.L., Hall, I.R., Zahn, R., Elderfield, H., Grousset, F., Hemming, S.R., Scourse, J.D., 2006. High resolution evidence for linkages between NW European ice sheet instability and Atlantic Meridional Overturning Circulation. Earth and Planetary Science Letters 243, 476-488.

Petersen, G.N., Bjornsson, H., Arason, P., von Löwis, S., 2012. Two weather radar time series of the altitude of the volcanic plume during the May 2011 eruption of Grímsvötn, Iceland. Earth System Science Data 4, 121-127.

Pilcher, J.R., Hall, V.A., 1992. Towards a tephrochronology for the Holocene of the north of Ireland. The Holocene 2, 255-259.

Ponomareva, V., Polyak, L., Portnyagin, M., Abbott, P.M., Zelenin, E., Garbe-Schönberg, D., Vakhrameeva, P., (in press) “Holocene tephra from the Chukchi-Alaskan margin, Arctic Ocean: Implications for sediment chronostratigraphy and volcanic history”, Quaternary Geochronology.

Pouget, S., Bursik, M., Rogova, G., 2014. Tephra redeposition and mixing in a Lateglacial hillside basin determined by fusion of clustering analyses of glass-shard geochemistry. Journal of Quaternary Science 29, 789-802.

Pyle, D.M., 1989. The thickness, volume and grainsize of tephra fall deposits. Bulletin of Volcanology 51, 1-15.

Pyne-O'Donnell, S.D.F., Hughes, P.D.M., Froese, D.G., Jensen, B.J.L., Kuehn, S.C., Mallon, G., Amesbury, M.J., Charman, D.J., Daley, T.J., Loader, N.J., Mauquoy, D., Street-Perrott, F.A., Woodman-Ralph, J., 2012. High-precision ultra-distal Holocene tephrochronology in North America. Quaternary Science Reviews 52, 6-11.

Rasmussen, T.L., Thomsen, E., Moros, M., 2016. North Atlantic warming during Dansgaard-Oeschger events synchronous with Antarctic warming and out-of-phase with Greenland climate. Scientific Reports 6, 20535.

Rebesco, M., Hernandez-Molina, F., J., Van Rooij, D., Wåhlin, A., 2014. Contourites and associated sediments controlled by deep-water circulation processes: State-of-the-art and future considerations. Marine Geology 352, 111-154.

Rose, N.L., Golding, P.N.E., Batterbee, R.W., 1996. Selective concentration and enumeration of tephra shards from lake sediment cores. Holocene 6, 243-246.

Ruddiman, W.F., Glover, L.K., 1972. Vertical mixing of ice-rafted volcanic ash in North Atlantic sediments. Geological Society Bulletin 83, 2817-2836.

Sparks, R.S.J., Wilson, L., Sigurdsson, H., 1981. The pyroclastic deposits of the 1875 eruption of Askja, Iceland. Philosophical Transactions of the Royal Society of London, Series A 299, 241-273.

Steinhauser, G., Bichler, M., 2008. Adsorption of ions onto high silica volcanic glass. Applied Radiation and Isotopes 66, 1-8.

Stoner, J.S., Channell, J.E.T., Hillaire-Marcel, C., Kissel, C., 2000. Geomagnetic paleointensity and environmental record from Labrador Sea core MD95-2024: global marine sediment and ice core chronostratigraphy for the last 110 kyr. Earth and Planetary Science Letters 183, 161-177.

Todd, J.A., Austin, W.E.N., Abbott, P.M., 2014. Quantifying bioturbation of a simulated ash fall event. In Austin, W.E.N., Abbott, P.M., Davies, S.M., Pearce, N.J.G., Wastegård, S., (eds) Marine Tephrochronology, Geological Society of London Special Publication 398, 195-207.

Turney, C.S.M., 1998. Extraction of rhyolitic component of Vedde microtephra from minerogenic lake sediments. Journal of Palaeolimnology 19, 199-206.

Voelker, A.H.L., Haflidason, H., 2015. Refining the Icelandic tephrachronology of the last glacial period – The deep-sea core PS2644 record from the southern Greenland Sea. Global and Planetary Change 131, 35-62.

Watson, E.J., Swindles, G.T., Lawson, I.T., Savov, I.P., 2015. Spatial variability of tephra and carbon accumulation in a Holocene peatland. Quaternary Science Reviews 124, 248-264.

Weinelt, M., Vogelsang, E., Kucera, M., Pflaumann, U., Sarnthein, M., Voelker, A., Erlenkeuser, H., Malmgren, B.A., 2003. Variability of North Atlantic heat transfer during MIS 2. Paleoceanography 18, 1071.

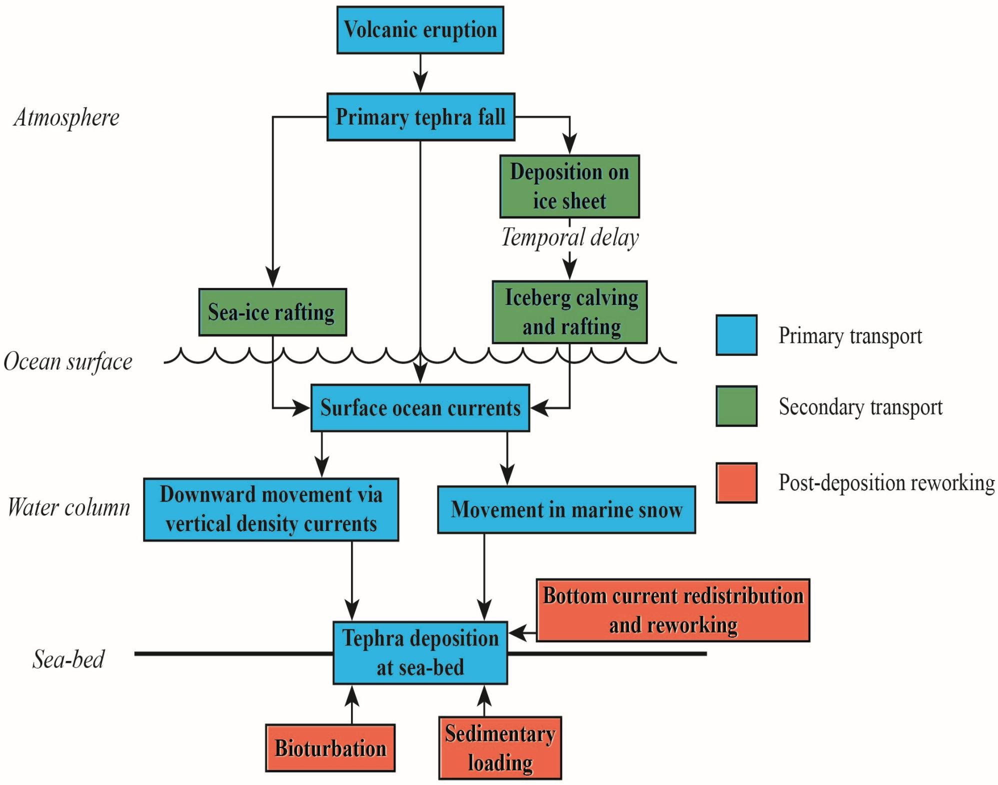
Volcanic eruption
Atmosphere
Primary tephra fall
Deposition on ice sheet
Temporal delay
Sea-ice rafting
Iceberg calving and rafting
Ocean surface
Surface ocean currents
Water column
Downward movement via vertical density currents
Movement in marine snow
Bottom current redistribution and reworking
Sea-bed
Tephra deposition at sea-bed
Bioturbation
Sedimentary loading
Primary transport
Secondary transport
Post-deposition reworking

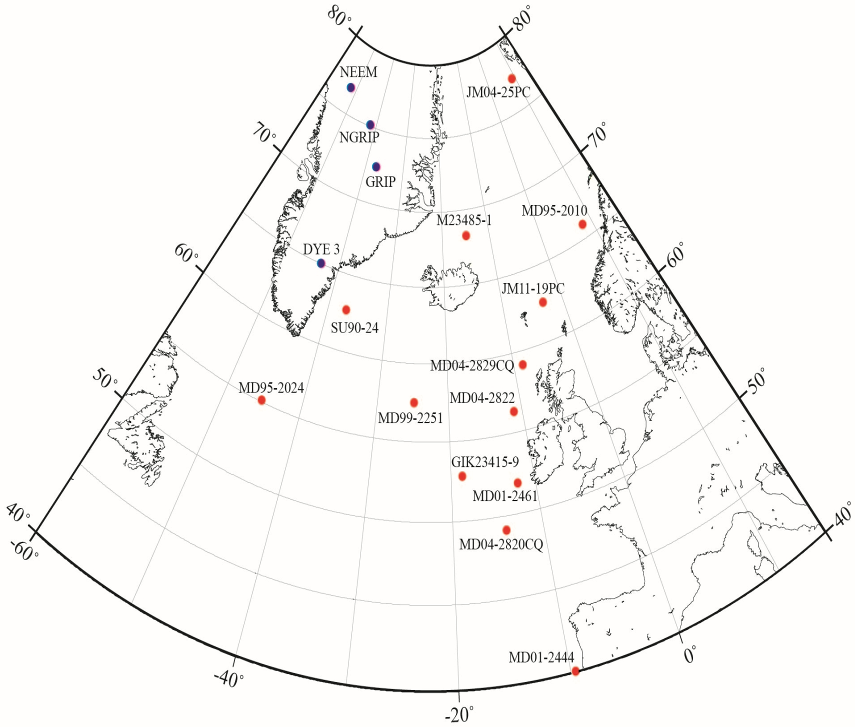

80°
80°
70°
70°
60°
60°
50°
50°
40°
40°
-60°
-40°
-20°
0°
NEEM
NGRIP
GRIP
DYE 3
SU90-24
MD95-2024
MD99-2251
JM04-25PC
M23485-1
MD95-2010
JM11-19PC
MD04-2829CQ
MD04-2822
GIK23415-9
MD01-2461
MD04-2820CQ
MD01-2444

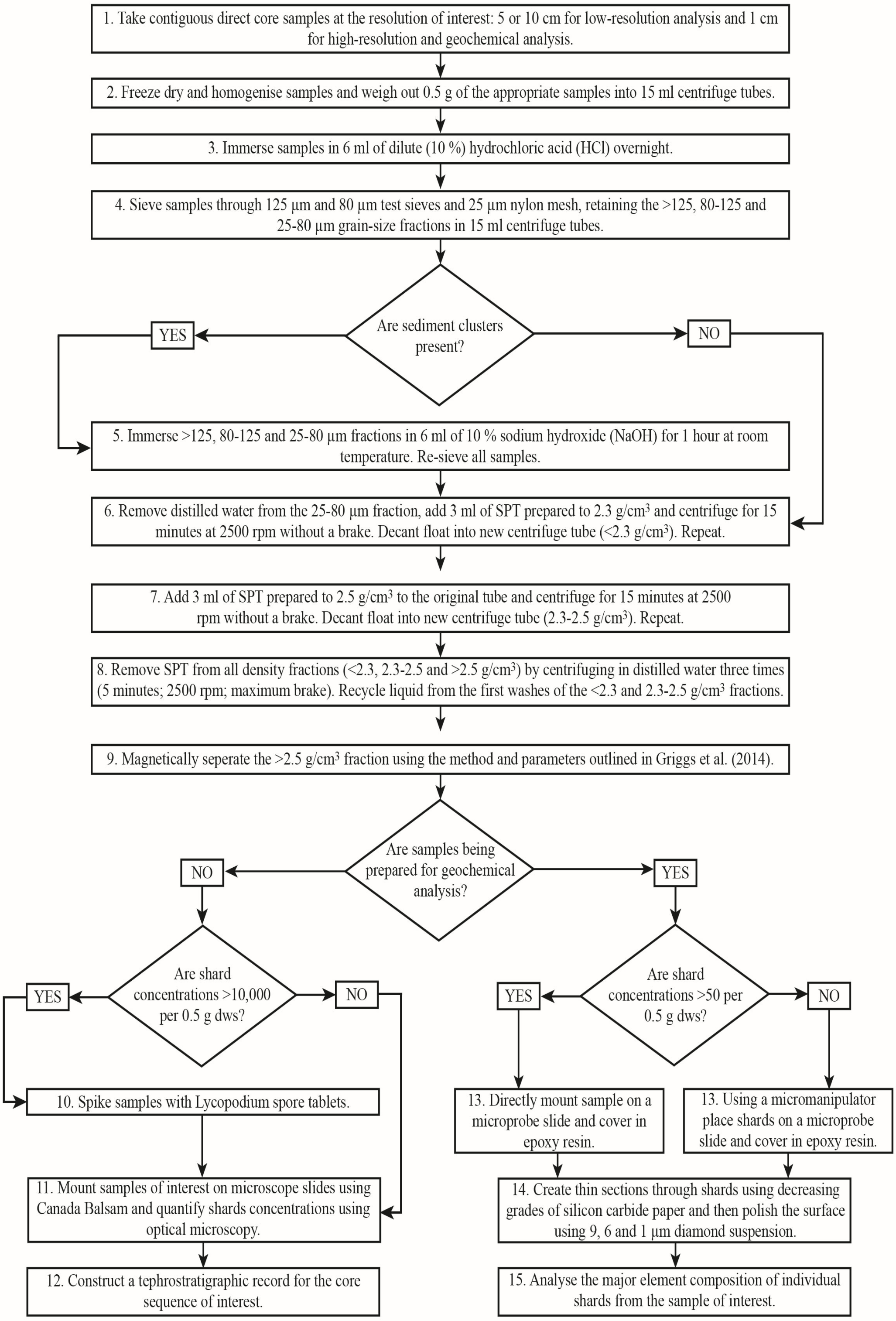
1. Take contiguous direct core samples at the resolution of interest: 5 or 10 cm for low-resolution analysis and 1 cm for high-resolution and geochemical analysis.
2. Freeze dry and homogenise samples and weigh out 0.5 g of the appropriate samples into 15 ml centrifuge tubes.
3. Immerse samples in 6 ml of dilute (10 %) hydrochloric acid (HCl) overnight.
4. Sieve samples through 125 µm and 80 µm test sieves and 25 µm nylon mesh, retaining the >125, 80-125 and 25-80 µm grain-size fractions in 15 ml centrifuge tubes.
Are sediment clusters present?
YES
NO
5. Immerse >125, 80-125 and 25-80 µm fractions in 6 ml of 10 % sodium hydroxide (NaOH) for 1 hour at room temperature. Re-sieve all samples.
6. Remove distilled water from the 25-80 µm fraction, add 3 ml of SPT prepared to 2.3 g/cm³ and centrifuge for 15 minutes at 2500 rpm without a brake. Decant float into new centrifuge tube (<2.3 g/cm³). Repeat.
7. Add 3 ml of SPT prepared to 2.5 g/cm³ to the original tube and centrifuge for 15 minutes at 2500 rpm without a brake. Decant float into new centrifuge tube (2.3-2.5 g/cm³). Repeat.
8. Remove SPT from all density fractions (<2.3, 2.3-2.5 and >2.5 g/cm³) by centrifuging in distilled water three times (5 minutes; 2500 rpm; maximum brake). Recycle liquid from the first washes of the <2.3 and 2.3-2.5 g/cm³ fractions.
9. Magnetically seperate the >2.5 g/cm³ fraction using the method and parameters outlined in Griggs et al. (2014).
Are samples being prepared for geochemical analysis?
NO
YES
Are shard concentrations >10,000 per 0.5 g dws?
YES
NO
Are shard concentrations >50 per 0.5 g dws?
YES
NO
10. Spike samples with Lycopodium spore tablets.
11. Mount samples of interest on microscope slides using Canada Balsam and quantify shards concentrations using optical microscopy.
12. Construct a tephrostratigraphic record for the core sequence of interest.
13. Directly mount sample on a microprobe slide and cover in epoxy resin.
13. Using a micromanipulator place shards on a microprobe slide and cover in epoxy resin.
14. Create thin sections through shards using decreasing grades of silicon carbide paper and then polish the surface using 9, 6 and 1 µm diamond suspension.
15. Analyse the major element composition of individual shards from the sample of interest.

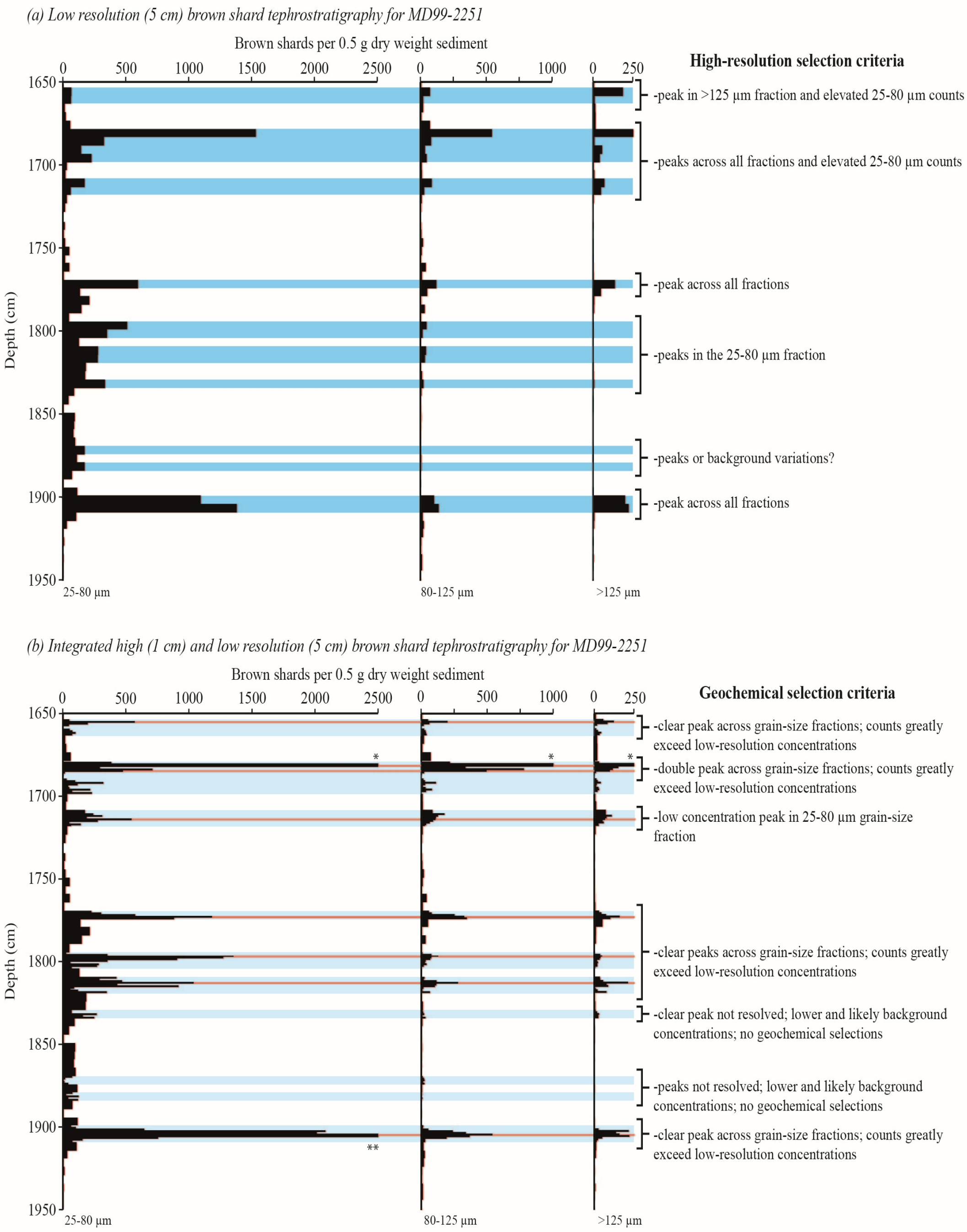
(a) Low resolution (5 cm) brown shard tephrostratigraphy for MD99-2251
Brown shards per 0.5 g dry weight sediment
0 500 1000 1500 2000 2500 0 500 1000 0 250
Depth (cm)
1650 1700 1750 1800 1850 1900 1950
25-80 µm
80-125 µm
>125 µm
High-resolution selection criteria
-peak in >125 µm fraction and elevated 25-80 µm counts
-peaks across all fractions and elevated 25-80 µm counts
-peak across all fractions
-peaks in the 25-80 µm fraction
-peaks or background variations?
-peak across all fractions
(b) Integrated high (1 cm) and low resolution (5 cm) brown shard tephrostratigraphy for MD99-2251
Brown shards per 0.5 g dry weight sediment
0 500 1000 1500 2000 2500 0 500 1000 0 250
Depth (cm)
1650 1700 1750 1800 1850 1900 1950
*
**
25-80 µm
80-125 µm
>125 µm
Geochemical selection criteria
-clear peak across grain-size fractions; counts greatly exceed low-resolution concentrations
-double peak across grain-size fractions; counts greatly exceed low-resolution concentrations
-low concentration peak in 25-80 µm grain-size fraction
-clear peaks across grain-size fractions; counts greatly exceed low-resolution concentrations
-clear peak not resolved; lower and likely background concentrations; no geochemical selections
-peaks not resolved; lower and likely background concentrations; no geochemical selections
-clear peak across grain-size fractions; counts greatly exceed low-resolution concentrations

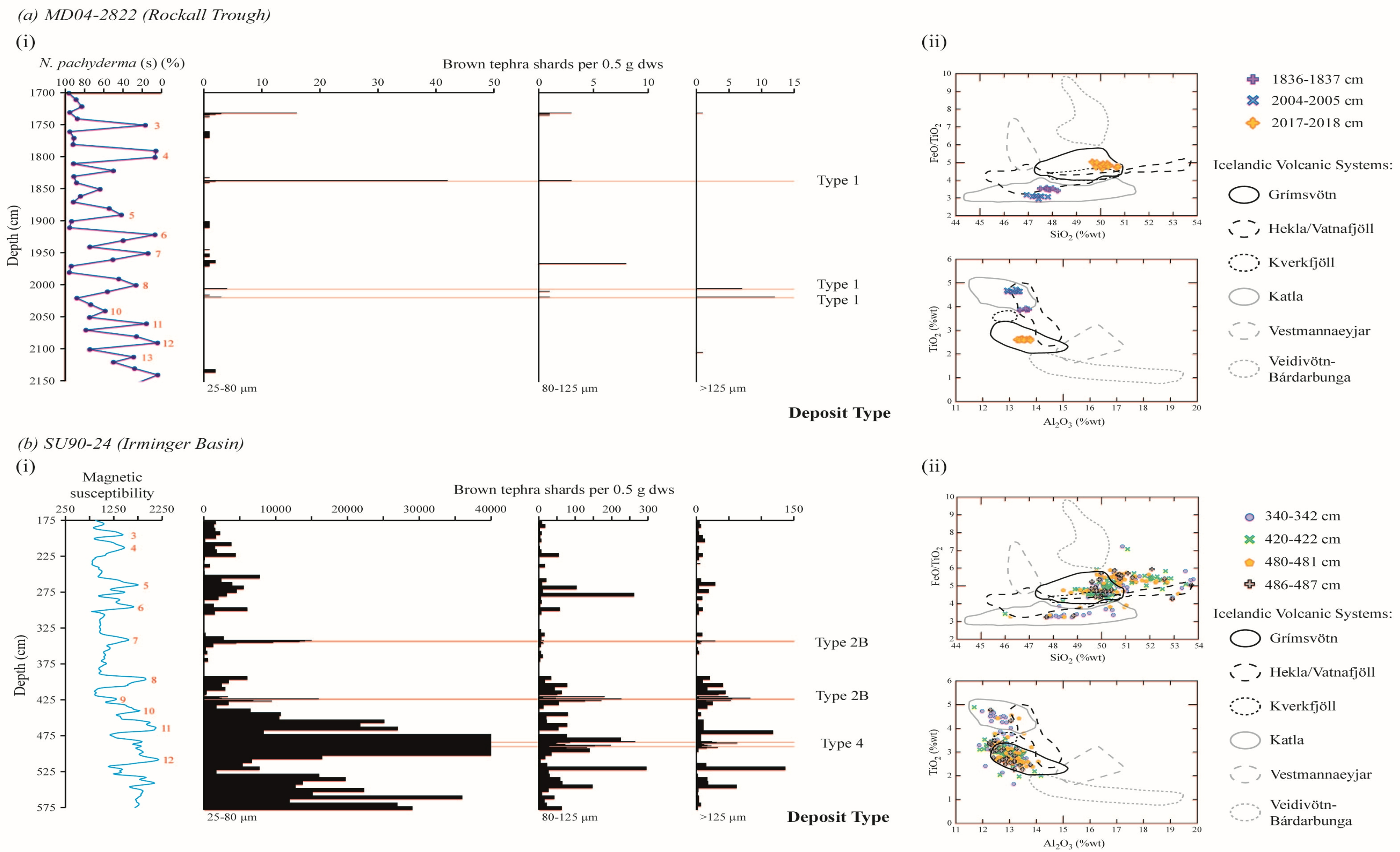
(a) MD04-2822 (Rockall Trough)
(i)
N. pachyderma (s) (%)
Depth (cm)
Brown tephra shards per 0.5 g dws
25-80 µm
80-125 µm
>125 µm
Type 1
Type 1
Type 1
Deposit Type
(ii)
1836-1837 cm
2004-2005 cm
2017-2018 cm
Icelandic Volcanic Systems:
Grímsvötn
Hekla/Vatnafjöll
Kverkfjöll
Katla
Vestmannaeyjar
Veidivötn-Bárdarbunga
FeO/TiO2
SiO2 (%wt)
TiO2 (%wt)
Al2O3 (%wt)
(b) SU90-24 (Irminger Basin)
(i)
Magnetic susceptibility
Depth (cm)
Brown tephra shards per 0.5 g dws
25-80 µm
80-125 µm
>125 µm
Type 2B
Type 2B
Type 4
Deposit Type
(ii)
340-342 cm
420-422 cm
480-481 cm
486-487 cm
Icelandic Volcanic Systems:
Grímsvötn
Hekla/Vatnafjöll
Kverkfjöll
Katla
Vestmannaeyjar
Veidivötn-Bárdarbunga

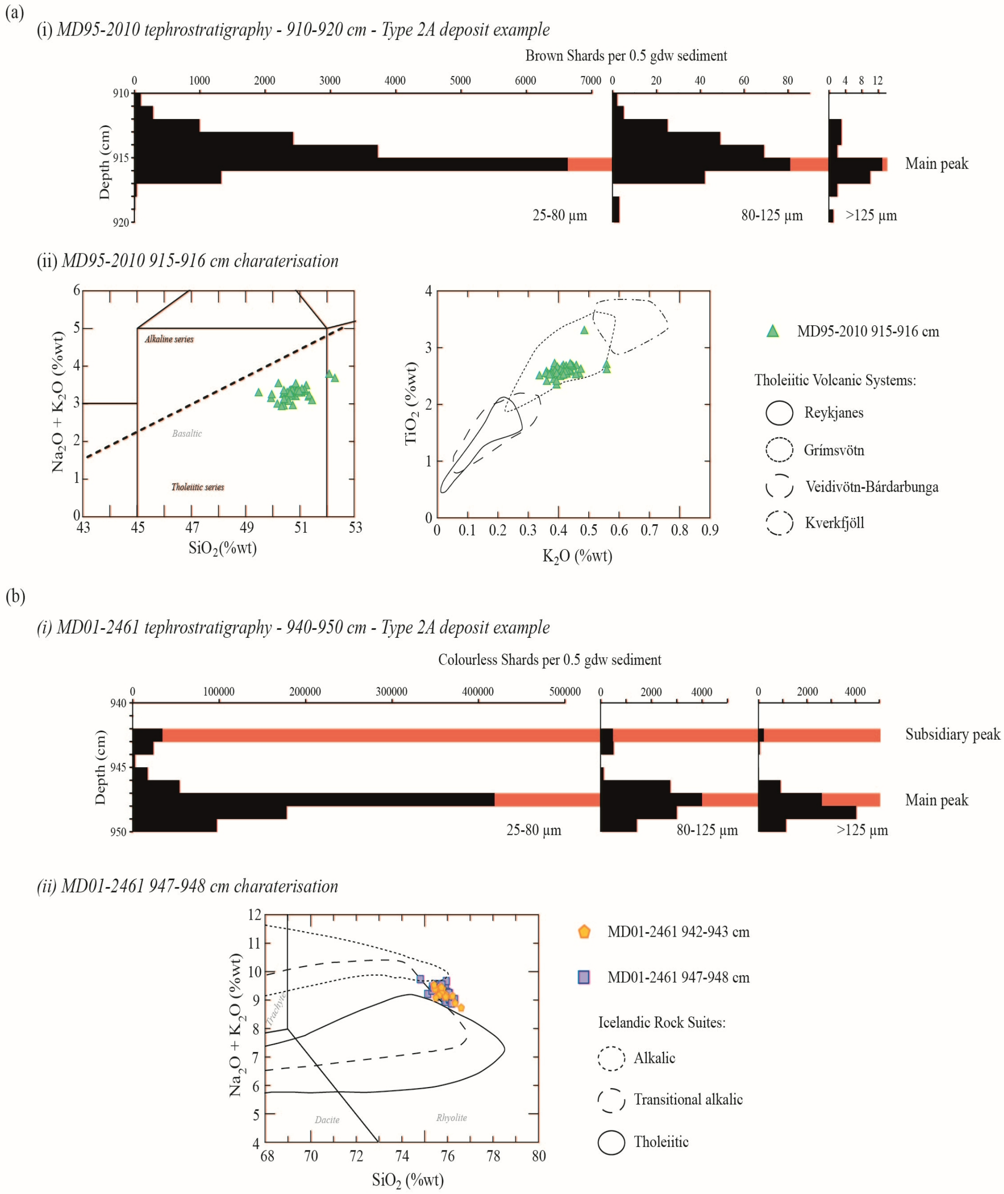
(a)
(i) MD95-2010 tephrostratigraphy - 910-920 cm - Type 2A deposit example
Brown Shards per 0.5 gdw sediment
Depth (cm)
Main peak
25-80 µm
80-125 µm
>125 µm
(ii) MD95-2010 915-916 cm charaterisation
Alkaline series
Basaltic
Tholeiitic series
Na2O + K2O (%wt)
SiO2(%wt)
TiO2 (%wt)
K2O (%wt)
MD95-2010 915-916 cm
Tholeiitic Volcanic Systems:
Reykjanes
Grímsvötn
Veidivötn-Bárdarbunga
Kverkfjöll
(b)
(i) MD01-2461 tephrostratigraphy - 940-950 cm - Type 2A deposit example
Colourless Shards per 0.5 gdw sediment
Depth (cm)
Subsidiary peak
Main peak
25-80 µm
80-125 µm
>125 µm
(ii) MD01-2461 947-948 cm charaterisation
Dacite
Rhyolite
Na2O + K2O (%wt)
SiO2 (%wt)
MD01-2461 942-943 cm
MD01-2461 947-948 cm
Icelandic Rock Suites:
Alkalic
Transitional alkalic
Tholeiitic

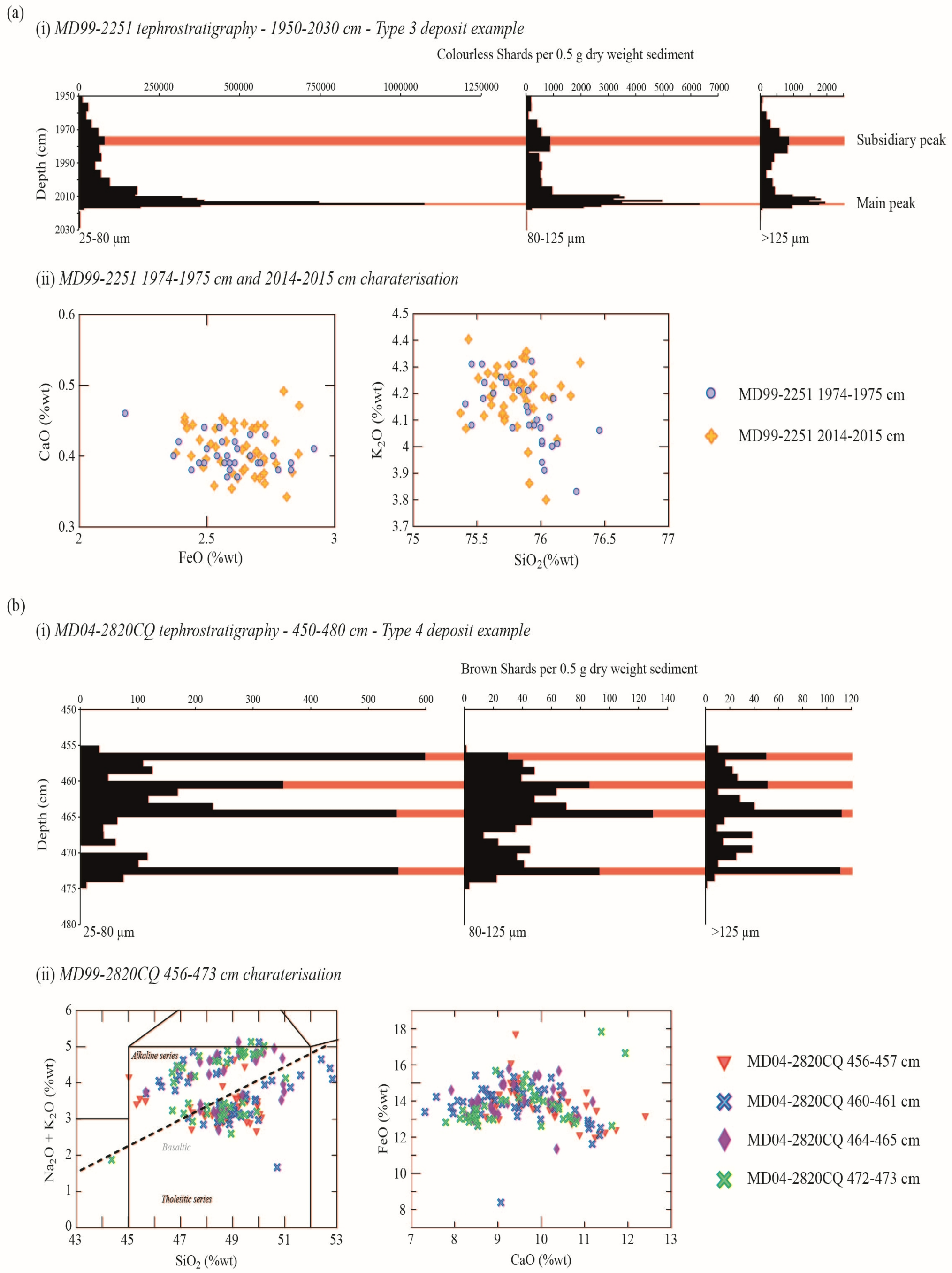
(a)
(i) MD99-2251 tephrostratigraphy - 1950-2030 cm - Type 3 deposit example
Colourless Shards per 0.5 g dry weight sediment
Depth (cm)
25-80 μm
80-125 μm
>125 μm
Subsidiary peak
Main peak
(ii) MD99-2251 1974-1975 cm and 2014-2015 cm charaterisation
CaO (%wt)
FeO (%wt)
K_2O (%wt)
SiO_2(%wt)
MD99-2251 1974-1975 cm
MD99-2251 2014-2015 cm
(b)
(i) MD04-2820CQ tephrostratigraphy - 450-480 cm - Type 4 deposit example
Brown Shards per 0.5 g dry weight sediment
Depth (cm)
25-80 μm
80-125 μm
>125 μm
(ii) MD99-2820CQ 456-473 cm charaterisation
$Na_2O + K_2O$ (%wt)
SiO_2 (%wt)
Alkaline series
Basaltic
Tholeiitic series
FeO (%wt)
CaO (%wt)
MD04-2820CQ 456-457 cm
MD04-2820CQ 460-461 cm
MD04-2820CQ 464-465 cm
MD04-2820CQ 472-473 cm

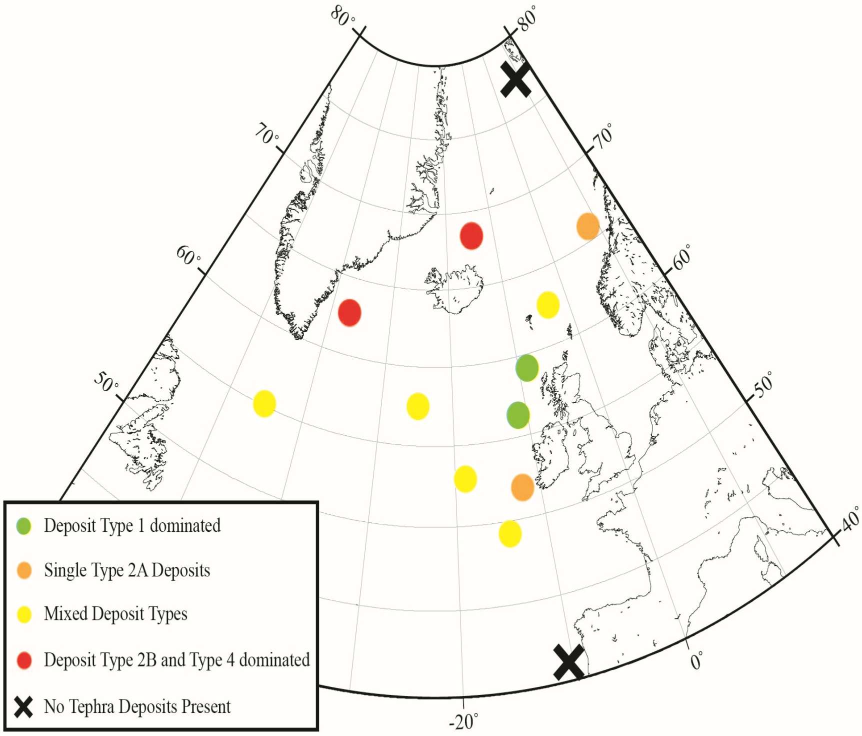

80°
80°
70°
70°
60°
60°
50°
50°
40°
0°
-20°
Deposit Type 1 dominated
Single Type 2A Deposits
Mixed Deposit Types
Deposit Type 2B and Type 4 dominated
No Tephra Deposits Present

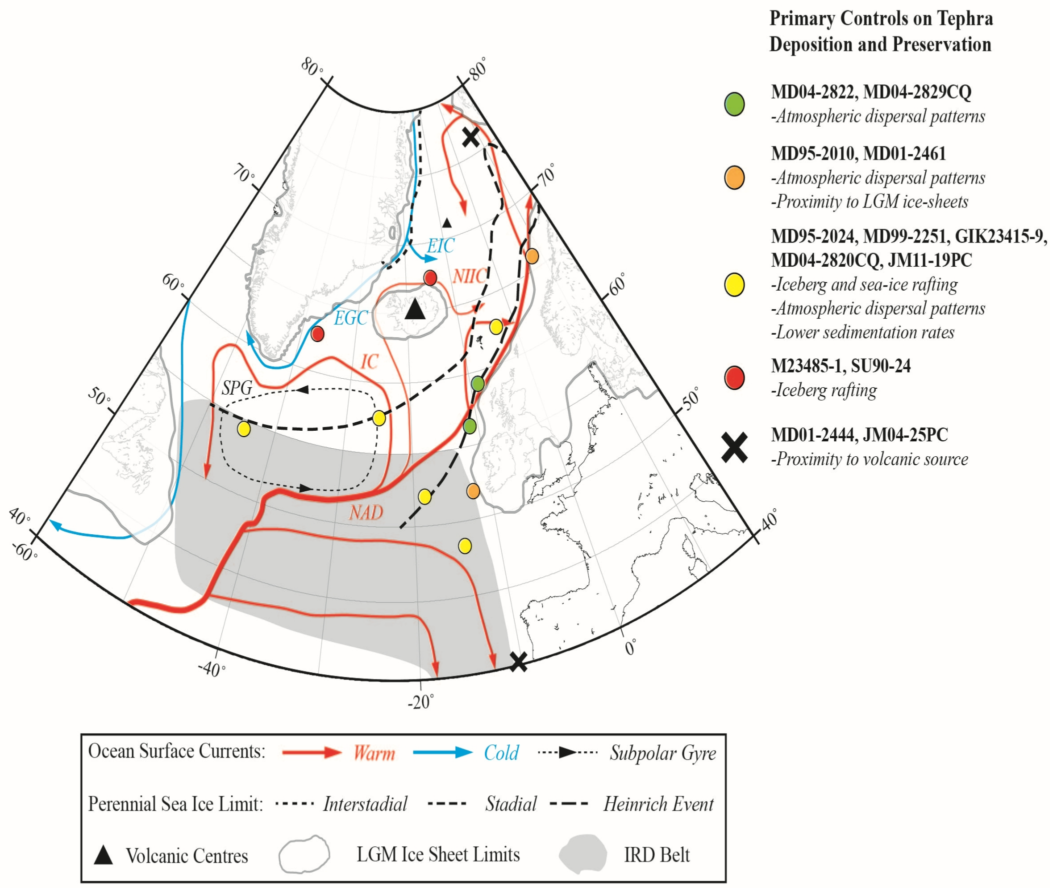
Primary Controls on Tephra Deposition and Preservation
MD04-2822, MD04-2829CQ
-Atmospheric dispersal patterns
MD95-2010, MD01-2461
-Atmospheric dispersal patterns
-Proximity to LGM ice-sheets
MD95-2024, MD99-2251, GIK23415-9, MD04-2820CQ, JM11-19PC
-Iceberg and sea-ice rafting
-Atmospheric dispersal patterns
-Lower sedimentation rates
M23485-1, SU90-24
-Iceberg rafting
MD01-2444, JM04-25PC
-Proximity to volcanic source
80°
80°
70°
70°
60°
60°
50°
50°
40°
40°
-60°
-40°
-20°
0°
EIC
NIIC
EGC
IC
SPG
NAD
Ocean Surface Currents: Warm Cold Subpolar Gyre
Perennial Sea Ice Limit: Interstadial Stadial Heinrich Event
Volcanic Centres
LGM Ice Sheet Limits
IRD Belt

Core	Location	Lat/Long	Water Depth	Approx. Average Sedimentation Rate (cm/ka)	Example References
JM04-25PC	Western Svalbard slope	77º 28′ N, 09º 30′ E	1880 m	10	Jessen et al. (2015)
M23485-1	Iceland Sea	76 º 54.9′ N, 17º 52.4′ W	1120 m	17	-
MD95-2010	Norwegian Sea	66º 41.05′ N, 04º 33.97′ E	1226 m	16	Dokken and Jansen (1999)
JM11-19PC	North Faroe Slope	62º 49′ N, 03º 52′ W	1179 m	11	Ezat et al. (2014); Griggs et al. (2014)
SU90-24	Irminger Basin	62º 40′ N, 37º 22′ W	2100 m	19	Elliot et al. (1998, 2001)
MD04-2829CQ	Rosemary Bank	58º 56.93′ N, 09º 34.30′ W	1743 m	20	Hall et al. (2011)
MD04-2822	Rockall Trough	56º 50.54′ N, 11º 22.96′ W	2344 m	14	Hibbert et al. (2010)
MD99-2251	Gardar Drift	57º 26′ N, 27º 54′ W	2620 m	11	-
MD95-2024	Labrador Sea	50º 12.40′ N, 45º 41.22′ W	3539 m	22	Stoner et al. (2000)
GIK23415-9	Northern North Atlantic	53º 10.7′ N, 19º 08.7′ W	2472 m	9	Weinelt et al. (2003)
MD01-2461	Porcupine Seabight	51º 45′ N, 12º 55′ W	1153 m	13	Peck et al. (2006, 2008)
MD04-2820CQ	Goban Spur	49º 05.29′ N, 13º 25.90′ W	3658 m	11	Abbott et al. (2016)
MD01-2444	Iberian Margin	37º 33.68′ N, 10º 08.53′ W	2637 m	23	Martrat et al. (2007)

Table 1: Details of the North Atlantic marine core network investigated in this study. Approximate sedimentation rates cover the 25-60 ka BP period for the cores, except for MD04-2829CQ which covers the 25-41 ka BP period, and were calculated using existing age-depth models for the sequences or approximated based on ages for event markers e.g. Heinrich events and North Atlantic Ash Zone II.

Deposit Type	Typical Shard Profile	Deposit Type Characteristics	Transport and Deposition Processes
TYPE 1 Low concentration peak	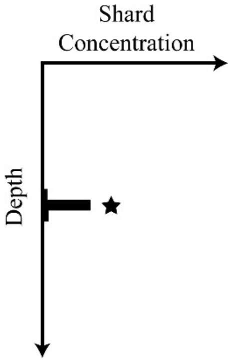	-Well constrained shard concentration peak -Low shard concentrations (< 50 per 0.5 g dws) -Shards generally 25-80 µm in diameter -Homogenous geochemical composition	-Single depositional event -Sourced from a single volcanic eruption -Potentially limited post-depositional reworking -Most likely primary airfall deposition
TYPE 2 High concentration peak	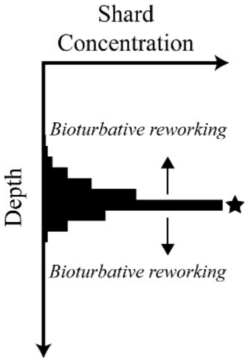	-Distinct peak in shard concentration -High shard concentrations (100s-1,000s per 0.5 g dws) -Upward and downward spanning up to 10 cm -Homogenous (Type 2A) or heterogeneous (Type 2B) geochemical composition	-Analysis of geochemistry, shard sizes and IRD required -Bioturbative reworking -Single depositional event -Transport via primary airfall, sea-ice and iceberg rafting possible
TYPE 3 High concentration peak; gradational upward tail	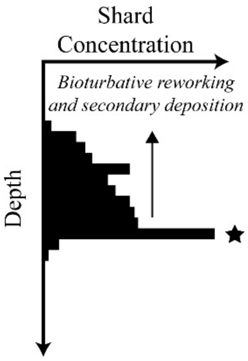	-Flat bottomed profile with a clear gradational upward tail -Very high shard concentrations (100,000s-1,000,000 per 0.5 g dws) -Deposit spread up to 100 cm -Homogenous composition of shards in peak	-Single depositional and volcanic event -Reworking via secondary deposition and bioturbation -Transport via primary airfall or sea-ice rafting -Useful isochron
TYPE 4 Diffuse distribution; multiple peaks	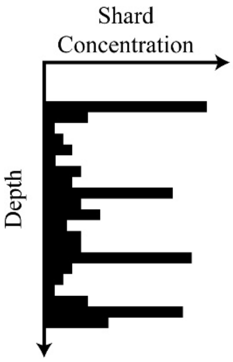	-High shard concentrations (1,000s-1,000,000s per 0.5 g dws) -Multiple peaks in concentration in a period of elevated shard concentrations -Deposit spread of 10s of cms -Heterogeneous geochemical composition common between peaks	-Deposition of multiple closely spaced eruptions or deposition via iceberg rafting -Comparison to Greenland tephra framework and IRD records required -Potential as regional marine-marine tie-lines
TYPE 5 Background of consistent concentration	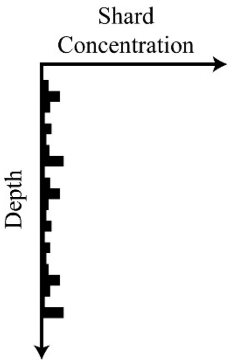	-Consistent deposition of shards with limited variability in concentrations between samples -Wide variability of deposit spreads -Heterogeneous or geochemically related to underlying deposits	-Background signal of glass shards -Shards reworked and remobilised in the oceanic system -Potential masking of low concentration tephra deposits

Table 2: Summary of the shard profiles, characteristics, transportation and deposition processes of tephra deposit types common to North Atlantic marine sequences between 25 and 60 ka BP. ★ = position of the isochron for that deposit type.